# A multi-component multi-temperature model for simulating laminar deflagration waves in mixtures of air and hydrogen

Olivier Hurisse

# A multi-component multi-temperature model for simulating laminar deflagration waves in mixtures of air and hydrogen.

Olivier Hurisse,
EDF Lab Chatou, 6 quai Watier, 78400 Chatou, France,
olivier.hurisse@edf.fr

January 17, 2023

**Abstract**

In this manuscript, a multi-component multi-temperature model is proposed for the simulation of laminar deflagration waves in mixtures of four gases: $H_2$, $0_2$, $N_2$ and $H_20$. The model is built following a thermodynamical approach and it inherits from several interesting mathematical properties: the model is hyperbolic, there is a unique solution for the Rankine-Hugoniot relations (i.e. for weak solutions / shock waves), the source terms are in agreement with the second law of thermodynamics. The correct propagation of the flame front is ensured by using the classical technique of the artificial thickening of the flame. Simple numerical schemes and classical methods are used for computing the approximated solutions of the model and for assessing its behavior on some basic test cases. The results are encouraging and further improvements should be done, in particular by modeling the effect of the turbulence on the front propagation.

**Keywords.** premixed laminar flame, hydrogen combustion, deflagration wave, multi-temperature model, artificial flame thickening.

## Contents

# 1 Introduction

The combustion of hydrogen is an industrial stake since several decades. It is involved in a lot of industrial processes for which its combustion gives rise to security issues. Moreover, the control of the combustion of hydrogen has raised an increasing interest for transport, for instance for propellers and vehicle engines. A good understanding of the complex reactive flows of hydrogen is a key point for designing efficient engines. In this domain, security is also an important point since the hydrogen is stored at high pressure in tanks that may be damaged, causing leaks which may lead to an explosion. This wide range of applications has led to an important effort in the physical modeling of hydrogen combustion [43, 21, 22, 7]. Following that theoretical works, the numerical simulation of $H_2$ combustion is investigated since several decades. As for many fields involving CFD, several different approaches have been tested: from the coarser ones generally dedicated to large industrial domains, to the most accurate ones actually restricted too small combustion rooms. The present work aims at presenting a multi-component multi-temperature model for laminar deflagration waves in hydrogen-air mixtures. It does not include the most finest physical models, in particular because the goal is to perform numerical simulation on large industrial domains for which simplified physics can be relevant. The building of the model is based on a thermodynamical point of view, which has already been successfully applied to propose multi-phase flows single-velocity models accounting for the thermodynamical disequilibrium [1, 34, 25].

The model proposed in this work is a multi-component model in the sense that the mixture of gases is composed of four gases $O_2$, $H_2$, $N_2$ and $H_2O$. We only consider water vapor here and not liquid water even if the modeling approach allows to take into account phase change and non-miscible phases, as proposed in [25]. For the model presented here, hydrogen-air mixtures are a particular case and more general mixtures can be dealt with. The mixture considered here is assumed to be an ideal mixing of miscible gases that are not at thermal equilibrium. Each gas is indeed described by its own temperature. As a consequence, the model contains one energy equation for each gas, which enables to account easily for the different diffusion coefficients of the gases [16, 15, 10]. These four energy equations appear in the model in the form of: one energy equation for the mixture and three equations for the convection of energy fractions. Therefore, few numerical complications are added by this assumption and we end up with a compressible Navier-Stokes system of equations supplemented by advection equations with source terms. The mass diffusivity is not taken into account in the model proposed here. For deflagration waves of premixed mixtures at industrial scales, this effect is not predominant. On the contrary, the thermal diffusion is mandatory in order to recover the correct speed of propagation of the flame as explained below.

The well-known one-step reaction $O_2 + 2H_2 \rightarrow 2H_2O$ for hydrogen oxidation shadows a far more complex chain of chemical reactions that produce and consume intermediate reaction-products [33, 31]. This complex thermochemistry strongly depends on the initial temperature and on the mass fractions of the gases in the mixture. It can be mandatory to account for this complete thermochemistry in order to numerically reproduce some very fine physical phenomenon which can not be predicted with the sole one-step reaction. This is the case for instance for all the situations involving autoignition processes of hydrogen [37]. In order to account for that complex chain of reactions, specific kinetic/chemical solvers, as Cantera [18] for instance, are used in the numerical codes dedicated to the fine simulation of combustion. Nevertheless, for the simulation of the ignition of gas clouds at an industrial scale, a one-step reaction may be sufficient. This choice has been made for instance in FLACS [19, 14] or P$^2$REMICS [12]. In the present work, the same assumption is made and the thermochemistry of the sole one-step reaction $O_2 + 2H_2 \rightarrow 2H_2O$ will be considered. Moreover, in the proposed model the reaction rate is modeled by an Arrhenius law. This feature is also classical and its interaction with thermal diffusion is essential for the model. In particular, the balance between the heat release due to the reaction and the heat conduction in the gases is a key point.

In standard conditions, the reaction $O_2 + 2H_2 \rightarrow H_2O$ is activated only if the temperature is high enough. Since it is an exothermic reaction, heat is released in the mixture when it occurs and the temperature of the burnt gases increases. In deflagration waves, this reaction zone is very thin and it corresponds to the front of the flame. The initial ignition of the reactants is ensured by a heat source, as a spark for instance. Afterwards, the propagation of the front of the deflagration flame in the mixture of gases is due to two mechanisms :

- the high temperature of the burnt gases that follows the heat release due to the combustion/reaction ;
- and the transfer of this heat to the fresh gases that are near the flame front.

If the temperature increase is sufficient, the heating of the unburnt gases near the front activates the reaction. The reactants are progressively consumed and transformed into burnt gases, making the flame front progressing from the burnt gases to the unburnt gases. The heat transfer from the burnt gases to the fresh unburnt gases is ensured by the heat conduction and by the turbulent mixing. In this work, we only consider heat conduction

and turbulence will be accounted for in a further work on the basis of turbulence models proposed in [13]. Thanks to this choice, the classical (and widely used) technique of the *artificial thickening of the flame* [3] will be used to obtain a correct prediction of the speed of propagation of the flame front. In this technique, the thermal diffusion coefficient may be increased for coarse meshes and the reaction rate inversely decreased. Indeed, for coarse meshes, the numerical diffusion prevails over the thermal diffusion, leading to a incorrect balance between heat conduction and reaction rate. The speed of propagation of the flame is then not recovered in the numerical simulations. The *artificial thickening of the flame* enables to recover the correct balance by increasing artificially the diffusion coefficient so that it prevails over the numerical diffusion. The reaction rate is thus decreased accordingly.

In a numerical point of view, very basic solutions have been chosen. Emphasis was placed on robust schemes with strong mathematical properties on unstructured meshes rather than on accuracy. We thus restrict here to explicit schemes that are first order in space and time. The behavior of the model can thus quickly be assessed with a reasonable effort for implementation. Obviously, if the model appears to be satisfactory, efforts should be put on implementing more accurate and sophisticated schemes: high-order schemes or semi-implicit pressure-correction schemes. If first-order explicit schemes are well-suited for flows at high Mach number, the latter class of schemes allows to be more accurate on low Mach flows that occurs for slow deflagrations. It should be noted that the thermal diffusion fluxes are also approximated through an explicit scheme. Indeed, with the technique of *the artificial thickening of the flame* the diffusion coefficient can be modified into a non-physical value. This allows to overcome the classical Fourier stability condition that arises when using explicit thermal fluxes.

Three test cases have been examined here. The first one concerns the comparison between the AICC[1] quantities estimated by the model and some experimental measurements. This first test can be seen as a mere validation of the choice of the EOS parameters and of the numerical computation of the reaction. The second test case is the most important one. The influence of the different parameters involved in the technique of the *artificial thickening of the flame* are studied in a one-dimensional setting. Some specific choices are made in order to recover the correct speed of propagation of the front. These specific parameters have then been used for simulating the explosion of a mixture of 40% of hydrogen in air in a two-dimensional vented box. This last test case mimics the DIMITRHY experimental facility [42].

The outline of the paper is the following. Section 2 presents the model in details. This includes the physical assumptions and the analysis of the mathematical properties of the system of partial derivative equations associated with the model. A standard thermodynamical point of view is adopted for building the model. The numerical schemes are described in section 3 and they are applied in section 4 on simple laminar test cases for assessing the capabilities of the model.

# 2 A multi-component multi-temperature model for hydrogen combustion

## 2.1 Building the model on thermodynamical basis

In this section, a four-component model is proposed for hydrogen combustion. The latter is modeled through a one-step irreversible reaction: $O_2 + 2\ H_2 \longrightarrow 2\ H_2O$, while $N_2$ remains chemically inert. Hydrogen combustion is in fact composed of far more reactions with intermediate reactants and products, see among many other references [33, 31]. There exists a large literature on that subject but for the targeted applications, a one-step reaction can be sufficient in most situations. The model is first built using extensive quantities in section 2.1.1 to 2.1.4, and it is then converted to intensive quantities in section 2.1.5. These first sections deal with the convective terms and with the chemical reaction. The operator for the thermal diffusion is added afterwards in section 2.1.6 by using the fact that gases may have different temperatures.

### 2.1.1 Thermodynamical setting and definitions

Let us consider four gases: dioxygen $O_2$, hydrogen $H_2$, water vapor $H_2O$ and nitrogen $N_2$, which will be respectively designed by the subscripts 1, 2, 3 and 4 in the following. Each gas is described by its volume $V_i$ (in $m^3$), its mass $M_i$ (in $kg$) and its energy $E_i$ (in $J$) ; and we assume that the thermodynamical behavior of each gas is given through an intensive entropy $s_i$ (in $J/K/kg$) defined with respect to the specific volume $V_i/M_i$ and

[1] *Adiabatic, Isochoric and Complete Combustion*

to the specific energy $E_i/M_i$ of the gas: $(V_i/M_i, E_i/M_i) \mapsto s_i(V_i/M_i, E_i/M_i)$. The entropy $s_i$ is supposed to fulfill the following properties.

- The entropy $s_i$ is strictly concave with respect to $(V_i/M_i, E_i/M_i)$.
- The entropy $s_i$ belongs to $\mathbb{C}^2((\mathbb{R}_*^+)^2)$.
- The partial derivative of $s_i$ with respect to the the specific energy is positive: $\dfrac{\partial s_i}{\partial E_i/M_i}_{|V_i/M_i} > 0$.

On the basis of $s_i$, let us introduce the extensive entropy $\eta_i$:

$$(V_i, M_i, E_i) \mapsto \eta_i(V_i, M_i, E_i) = M_i s_i(V_i/M_i, E_i/M_i), \quad (\text{in } J/K) \quad .$$

The extensive entropy $\eta_i$ inherits from the properties of $s_i$.

**Proposition 2.1** *The entropy $\eta_i$ inherits several properties from the entropy $s_i$.*

*(i) The entropy $\eta_i$ is strictly concave with respect to $(V_i, M_i, E_i)$.*

*(ii) The entropy $\eta_i$ belongs to $\mathbb{C}^2((\mathbb{R}_*^+)^3)$.*

*(iii) The partial derivative of $\eta_i$ with respect to the the energy is positive: $\dfrac{\partial s_i}{\partial E_i}_{|V_i,M_i} > 0$.*

The proof of items *(ii)* and *(iii)* of proposition 2.1 and proposition 2.2 are straightforward. The proof of item *(i)* of proposition 2.1 can be found in appendix 6.1. Moreover, thanks to the form of $\eta_i$, the additional property holds:

**Proposition 2.2** *The entropy $\eta_i$ is positive homogeneous of degree 1 (PH1); for any $a > 0$ we have:*

$$\eta_i(aV_i, aM_i, aE_i) = a\eta_i(V_i, M_i, E_i).$$

It should be noted that the property described in proposition 2.2 is directly linked with the extensive form chosen for the entropy $\eta_i$. Its proof is straightforward.

The Classical Irreversible Thermodynamics assumption is made, which allows to define the Gibbs relation within phase $i$ as:

$$T_i d\eta_i = dE_i + P_i dV_i - G_i dM_i \tag{1}$$

Thanks to Gibbs relation (1), the pressure $P_i$ (in $Pa$), the temperature $T_i$ (in $K$) and the Gibbs enthalpy $G_i$ (in $J/kg$) can be defined for each gas on the basis on the entropy $\eta_i$:

$$\frac{P_i}{T_i} = \frac{\partial \eta_i}{\partial V_i}_{|M_i,E_i} \tag{2}$$

$$\frac{1}{T_i} = \frac{\partial \eta_i}{\partial E_i}_{|V_i,M_i} \tag{3}$$

$$\frac{G_i}{T_i} = \frac{\partial \eta_i}{\partial M_i}_{|V_i,E_i} \tag{4}$$

The Gibbs enthalpy reads $G_i = E_i/M_i + P_i \times V_i/M_i - T_i \times \eta_i/M_i$ and it is worth noting that it corresponds to an intensive quantity. The thermodynamical behavior of each gas is then completely defined. Let us turn now to the definition of the mixture of these gases.

Let us assume that the four gases are miscible and that it implies that they all occupy the same volume $V$:

$$\forall i, \quad V_i = V.$$

This miscibility constraint is classical even if other ones have been proposed in the literature. The mass $M$, the energy $E$ and the entropy $\eta$ of the mixture of gases are respectively defined as the sum of the partial masses, the sum of the partial energies, and the sum of the partial entropies:

$$M = \sum_{i=1}^{4} M_i, \quad E = \sum_{i=1}^{4} E_i, \quad \text{and} \quad \eta = \sum_{i=1}^{4} \eta_i.$$

It can be proved that the mixture entropy $\eta$ defined here possesses several concavity properties depending of the set of variables considered.

**Proposition 2.3** *The mixture entropy $\eta$ possesses the following properties:*

*(i) $\eta$ is concave (but not strictly) with respect to $(Vi, Mi, Ei)_{i=1..4}$;*

*(ii) $\eta/M$ is strictly concave with respect to $(V/M, E/M)$ for fixed $(M_i/M, E_i/E)$;*

*(iii) $\eta/M$ is strictly concave with respect to $(M_i/M, E_i/E)$ for fixed $(V, M, E)$.*

Detailed proofs for proposition (2.3) may be found in appendix 6.1.

By differentiating the mixture entropy $\eta$ and by using the Gibbs relations for each gas (1), one straightforwardly gets:

$$d\eta = \sum_{i=1}^{4} \left( \frac{1}{T_i} dE_i + \frac{P_i}{T_i} dV_i - \frac{G_i}{T_i} dM_i \right) \tag{5}$$

For any quantity $\Phi_i = \{V_i, M_i, E_i\}$ with $\Phi = \sum_{i=1}^{4} \Phi_i$, the following simple calculus holds:

$$d\Phi_i = \frac{\Phi_i}{\Phi}\ d\Phi - \Phi\ d\left(\frac{\Phi_i}{\Phi}\right). \tag{6}$$

It should be noticed that by summing relation (6) over $i = 1..4$, we also get:

$$\sum_{i=1}^{4} d\left(\frac{\Phi_i}{\Phi}\right) = 0. \tag{7}$$

When introducing relation (6) into equation (5), the latter can be written:

$$d\eta = \sum_{i=1}^{4} \left( \frac{E_i}{E} \frac{1}{T_i} \right) dE + \sum_{i=1}^{4} \left( \frac{V_i}{V} \frac{P_i}{T_i} \right) dV + \sum_{i=1}^{4} \left( \frac{M_i}{M} \frac{G_i}{T_i} \right) dM$$
$$+E \sum_{i=1}^{4} \left( \frac{1}{T_i} d\left(\frac{E_i}{E}\right) \right) + V \sum_{i=1}^{4} \left( \frac{P_i}{T_i} d\left(\frac{V_i}{V}\right) \right) + M \sum_{i=1}^{4} \left( \frac{G_i}{T_i} d\left(\frac{M_i}{M}\right) \right)$$

This relation corresponds to the general Gibbs relation for a mixture of four components. The first three terms on the right hand side correspond to exchanges of mass, volume and energy between the mixture and its surrounding ; while the last three terms rules the internal exchanges between the four components. From this mixture Gibbs relation, a mixture temperature $T$ , a mixture pressure $P$ and a mixture Gibbs enthalpy $G$ can be defined as:

$$\frac{1}{T} = \sum_{i=1}^{4} \left( \frac{E_i}{E} \frac{1}{T_i} \right), \quad \frac{P}{T} = \sum_{i=1}^{4} \left( \frac{V_i}{V} \frac{P_i}{T_i} \right), \quad \text{and} \quad \frac{G}{T} = \sum_{i=1}^{4} \left( \frac{M_i}{M} \frac{G_i}{T_i} \right).$$

Introducing the miscibility constraint $V_i = V$ leads to the relations $V_i/V = 1$ and $d(V_i/V) = 0$, which gives the mixture Gibbs relation:

$$d\eta = \frac{1}{T} dE + \frac{P}{T} dV + \frac{G}{T} dM + E \sum_{i=1}^{4} \left( \frac{1}{T_i} d\left(\frac{E_i}{E}\right) \right) + M \sum_{i=1}^{4} \left( \frac{G_i}{T_i} d\left(\frac{M_i}{M}\right) \right), \tag{8}$$

with the mixture quantities defined as:

$$\frac{1}{T} = \sum_{i=1}^{4} \left( \frac{E_i}{E} \frac{1}{T_i} \right), \quad \frac{P}{T} = \sum_{i=1}^{4} \left( \frac{P_i}{T_i} \right), \quad \text{and} \quad \frac{G}{T} = \sum_{i=1}^{4} \left( \frac{M_i}{M} \frac{G_i}{T_i} \right). \tag{9}$$

It should be noticed that, when the four gases are at thermal equilibrium $T_i = T$, $\forall i$, the second relation in set (9) allows to recover the classical Dalton's law which states that: for an ideal mixture of miscible gases the mixture pressure is equal to the sum of the partial pressures, that is $P = \sum_{i=1}^{4} P_i$. In fact, by choosing the mixture entropy as: $\eta = \sum_{i=1}^{4} \eta_i$, an ideal mixing of the components has been assumed.

From the entropies of the four gases and from the Gibbs relations (1), the thermodynamical behavior of the mixture of the four gases has thus been defined. Indeed, the Gibbs relation for the mixture has been exhibited allowing to define the temperature of the mixture, the pressure of the mixture and the Gibbs enthalpy of the mixture. It now remains to account for the chemical reaction between the gases.

### 2.1.2 Accounting for the chemical reaction

We consider here the one-step chemical reaction for hydrogen combustion:

$$O_2 + 2\ H_2 \longrightarrow 2\ H_2O, \tag{10}$$

where the nitrogen $N_2$ is chemically inert. This means that $N_2$ does not participate in the reaction in a chemical point of view, but it will be seen in the following sections that it nonetheless plays a role in the overall thermo-chemistry of the mixture. Let us introduce the amount of moles of component $i$ denoted by $\mathcal{N}_i$ (in $mol$), and the molar mass of component $i$ denoted by $\mathcal{M}_i$ (in $kg/mol$). The latter is obviously a constant and we have the straightforward relation with the mass: $M_i = \mathcal{N}_i\mathcal{M}_i$. From reaction (10) we get the following relations between the amounts of moles:

$$\underbrace{\underbrace{d\mathcal{N}_1}_{O_2} + 2\underbrace{d\mathcal{N}_2}_{H_2}}_{\text{reactants}} = \underbrace{-2\underbrace{d\mathcal{N}_3}_{H_2O}}_{\text{product}}, \quad \text{and} \quad \underbrace{d\mathcal{N}_4}_{N_2} = 0. \tag{11}$$

By using the molar masses, system (11) can easily be converted into relations for the masses:

$$\frac{1}{\mathcal{M}_1}dM_1 + \frac{2}{\mathcal{M}_2}dM_2 = -\frac{2}{\mathcal{M}_3}dM_3, \quad \text{and} \quad dM_4 = 0. \tag{12}$$

Let us now assume that there is no mass exchange between the mixture and its surrounding, $dM = 0$. The definition of the mass of the mixture gives $\sum_{i=1}^{4} dM_i = dM = 0$. In addition to equations (12) the following system of equations can be formed:

$$\left\{ \begin{array}{l} dM_4 = 0, \\ \frac{1}{\mathcal{M}_1}dM_1 + \frac{2}{\mathcal{M}_2}dM_2 + \frac{2}{\mathcal{M}_3}dM_3 = 0, \\ dM_1 + dM_2 + dM_3 + dM_4 = dM. \end{array} \right. \tag{13}$$

If we define the constant $K$ as:

$$K = -\ \frac{\frac{1}{\mathcal{M}_1} - \frac{2}{\mathcal{M}_3}}{\frac{2}{\mathcal{M}_2} - \frac{2}{\mathcal{M}_3}},$$

system of equations (13) can be simplified in:

$$\left\{ \begin{array}{l} dM_4 = 0, \\ dM_3 = -(K+1)\ dM_1, \\ dM_2 = K\ dM_1. \end{array} \right. \tag{14}$$

It should be noted that $K$ is a dimensionless constant which only depends on the molar masses of $O_2$, $H_2$ and $H_2O$. With the classical values:

$$\mathcal{M}_1 = 31.9988\ 10^{-3}\ kg/mole, \quad \mathcal{M}_2 = 2.01588\ 10^{-3}\ kg/mole, \quad \text{and} \quad \mathcal{M}_3 = 18.01528\ 10^{-3}\ kg/mole,$$

we obtain $K \sim 0.0905$ which means that $K > 0$ and $(K+1) > 0$ in the second and third equations of system (14).

### 2.1.3 Definition of the thermo-chemical equilibrium state

In section 2.1.1 and in section 2.1.2, the thermodynamical behavior and the relations issued from the chemical reaction have been respectively defined. These two aspects are coupled in the present section by considering the thermo-chemistry of the mixture. For that purpose, we still consider that the mixture is a closed system for the mass, i.e. $dM = 0$, as introduced in section 2.1.2. Moreover, it is assumed that the energy and the volume of the mixture are constant: $dE = dV = 0$. Even if an adiabatic and isochoric reaction is considered here for modeling purpose, it is important to quote that the final model (see section 2.1.5) is not restricted to this mere configurations. In the complete model defined in section 2.1.5, exchanges through mass and energy fluxes are possible between the different elementary systems through the Euler system.

For an isolated, adiabatic and isochoric system, Gibbs relation (8) for the mixture can be simplified and it only contains the terms that are associated with the internal exchanges between the four gases. It indeed simply reads now:

$$d\eta = E\sum_{i=1}^{4}\left(\frac{1}{T_i}d\left(\frac{E_i}{E}\right)\right) + M\sum_{i=1}^{4}\left(\frac{G_i}{T_i}d\left(\frac{M_i}{M}\right)\right). \tag{15}$$

Then, using relation (7) and introducing the second and the third equations of system (14) into equation (15), we obtain:

$$d\eta = E\sum_{i=1}^{3}\left(\frac{1}{T_i}-\frac{1}{T_4}\right)d\left(\frac{E_i}{E}\right)+M\left(\frac{G_1}{T_1}+K\frac{G_2}{T_2}-(K+1)\frac{G_3}{T_3}\right)d\left(\frac{M_1}{M}\right). \tag{16}$$

We are interested now in the properties of proposition 2.3, in particular the third one (item (*iii*)). The second law of thermodynamics applied to a closed and isolated system states that the concave mixture entropy must increase: $d\eta \geq 0$, and that it can reach an asymptotic equilibrium state which is defined as the maximum of the entropy $\eta$. Since the latter is strictly concave for fixed $(V, M, E)$, this equilibrium state is unique. Let us denote the equilibrium state by: $\overline{M}_i$ and $\overline{E}_i$, for $i = 1..4$, which is uniquely defined for a given $(V, M, E)$ as:

$$\eta((V,\overline{M}_i,\overline{E}_i)_{i=1..4}) = \max_{\mathcal{A}_{eq}(V,M,E)}\left(\eta((V,M_i,E_i)_{i=1..4})\right), \tag{17}$$

with:

$$\mathcal{A}_{eq}(V,M,E) = \left\{(V,M_i,E_i)_{i=1..4} \;/\; \sum_{i=1}^{4}M_i = M, \sum_{i=1}^{4}E_i = E_{i=1..4}\right\}.$$

When all the components are present, the first order conditions for the optimality of equilibrium state are given by the partial derivative of $\eta$ with respect to $M_1/M$, $E_1/E$, $E_2/E$ and $E_3/E$. They can be obtained easily thanks to the Gibbs relation (16):

$$\left\{\begin{array}{l} T_i(V,\overline{M}_i,\overline{E}_i) = T_4(V,\overline{M_4},\overline{E_4}),\ \forall i = 1..3, \\ G_1(V,\overline{M}_1,\overline{E}_1) + KG_2(V,\overline{M}_2,\overline{E}_2) - (K+1)G_3(V,\overline{M}_3,\overline{E}_3) = 0, \\ E = \sum_{i=1}^{4}\overline{E}_i, \\ M = \sum_{i=1}^{4}\overline{M}_i, \end{array}\right. \tag{18}$$

where the last two relations in (18) are respectively the conservation of energy and mass which arise from the constraint $dE = 0$ and $dM = 0$.

System (18) is not closed, it is composed of 6 equations for the 8 unknowns $\overline{M}_i$ and $\overline{E}_i$ for $i = 1..4$. It should be recalled that $V$, $M$, $E$ and $K$ are constants here. The two missing relations are those pertaining to system (14), which describes the exchange of mass due to the chemical reaction. Indeed, let us assume an initial state with given $M_i$ and $E_i$ for $i = 1..4$. System (14) holds for all the thermodynamical path between $(M_i, E_i)_{i=1..4}$ and the asymptotic equilibrium state $(\overline{M}_i, \overline{E}_i)_{i=1..4}$, and - since $K$ is a constant - equations of system (14) can be integrated into:

$$\left\{\begin{array}{l} \overline{M}_4 = M_4, \\ (\overline{M}_3 - M_3) = -(K+1)\ (\overline{M}_1 - M_1), \\ (\overline{M}_2 - M_2) = K\ (\overline{M}_1 - M_1). \end{array}\right. \tag{19}$$

When gas 2 is completely consumed by the reaction (gas 1 is in excess), we get: $\overline{M}_2 = 0$, and the third equation of system (19) gives: $\overline{M}_1 = M_1 - M_2/K$. On the contrary, when there is no gas 3 at the end of the reaction, $\overline{M}_3 = 0$, we get from the second equation of (19) that: $\overline{M}_1 = M_1 + M_3/(K+1)$. Hence the mass $\overline{M}_1$ belongs to the interval:

$$\mathcal{I}_{\overline{M}_1} = \left[\max\left(0, M_1 - \frac{M_2}{K}\right); \min\left(1, M_1 + \frac{M_3}{K+1}\right)\right]. \tag{20}$$

It should be noted that since $K > 0$, $M_1 \in \mathcal{I}_{\overline{M}_1}$, so that the case without reaction $\overline{M}_1 = M_1$ belongs to the range of equilibrium defined by $\mathcal{I}_{\overline{M}_1}$.

Remembering that the mass conservation $M = \sum_{i=1}^{4}\overline{M}_i$ has already been accounted for in system (14), and thus in system (19), we can merge the latter with system (18) to obtain a closed system of equations that defines the equilibrium state $(\overline{M}_i, \overline{E}_i)_{i=1..4}$:

$$\left\{\begin{array}{l} T_i(V,\overline{M}_i,\overline{E}_i) = T_4(V,\overline{M}_4,\overline{E}_4),\ \forall i = 1..3, \\ G_1(V,\overline{M}_1,\overline{E}_1) + KG_2(V,\overline{M}_2,\overline{E}_2) - (K+1)G_3(V,\overline{M}_3,\overline{E}_3) = 0, \\ E = \sum_{i=1}^{4}\overline{E}_i, \\ \overline{M}_4 = M_4, \\ (\overline{M}_3 - M_3) = -(K+1)\ (\overline{M}_1 - M_1), \\ (\overline{M}_2 - M_2) = K\ (\overline{M}_1 - M_1). \end{array}\right. \tag{21}$$

where:

- $V$ is given and constant,
- $K$ is a given constant that only depends on the molar masses of the gases
- and where the initial state $(M_i, E_i)_{i=1..4}$ are given, and thus $E = \sum_{i=1}^4 E_i$ and $M = \sum_{i=1}^4 M_i$ are also known.

System (21) is a non-linear system of equations that gives the equilibrium state corresponding to an initial mixture of the four gases. This asymptotic state corresponds to the state reached for a fixed mixture volume, mass and energy which corresponds to the so-called *Adiabatic Isochoric and Complete Combustion* (AICC) state (see also section 4.1 for comparisons between numerical results of AICC state computations and experimental measurements). When system (21) has no solution, this means that the reaction is not possible. In other words, the mixture does not belong to the flammability domain and sole the thermal equilibrium between the gases has to be considered as explained below (see system (24) and associated explanations).

**Remark.** *It should be noted that we have* $E = \sum_{i=1}^4 E_i = \sum_{i=1}^4 \overline{E}_i$ *and* $M = \sum_{i=1}^4 M_i = \sum_{i=1}^4 \overline{M}_i$.

System (21) describes the equililbrium state that can be reached when the four components are present. When one or more components are missing, this equilibrium state is defined using a subset of the set of equations of system (21). Three representative examples are given below. When $N_2$ is not present, the system of equations that defines the equilibrium state is:

$$\left\{\begin{array}{l} T_1(V,\overline{M}_1,\overline{E}_1) = T_2(V,\overline{M}_2,\overline{E}_2) = T_3(V,\overline{M}_3,\overline{E}_3), \\ G_1(V,\overline{M}_1,\overline{E}_1) + KG_2(V,\overline{M}_2,\overline{E}_2) - (K+1)G_3(V,\overline{M}_3,\overline{E}_3) = 0, \\ E = \sum_{i=1}^3 \overline{E}_i, \\ (\overline{M}_3 - M_3) = -(K+1)\ (\overline{M}_1 - M_1), \\ (\overline{M}_2 - M_2) = K\ (\overline{M}_1 - M_1). \end{array}\right. \tag{22}$$

System (22) contains 6 equations for the 6 unknowns $(\overline{M}_i, \overline{E}_i)_{i=1..3}$. If one of the reactant is not present in the mixture, the chemical reaction is no more possible and we only have to account for the thermal disequilibrium. If one consider for instance that $O_2$ is missing, the equilibrium state is then defined through:

$$\left\{\begin{array}{l} T_2(V,\overline{M}_2,\overline{E}_2) = T_3(V,\overline{M}_3,\overline{E}_3) = T_4(V,\overline{M}_4,\overline{E}_4), \\ E = \sum_{i=2}^4 \overline{E}_i, \\ \overline{M}_i = M_i,\ \forall i = 2..4. \end{array}\right. \tag{23}$$

At last, we describe here a specific but important case. When the mixture does not belong to the flammability domain, reaction does not occur. It should be emphasized that in the present model the limits of the flammability domain arise from the EOS that have been chosen and from the computation of the equilibrium state (21). Indeed, if all the reactant are present and if system (21) has no solution, this means that the reaction can not occur. In such cases, it can be nonetheless necessary to ensure the return to the thermal equilibrium. Indeed, the latter occurs even if the chemical reaction is not possible. When the four gases are present, this thermal equilibrium is defined through the system:

$$\left\{\begin{array}{l} T_i(V,\overline{M}_i,\overline{E}_i) = T_4(V,\overline{M}_4,\overline{E}_4),\ \forall i = 1..3, \\ E = \sum_{i=2}^4 \overline{E}_i, \\ \overline{M}_i = M_i,\ \forall i = 2..4. \end{array}\right. \tag{24}$$

### 2.1.4 BGK source terms for modeling the thermal disequilibrium and the chemical reaction

It has been shown in section 2.1.3, that the mixture entropy $\eta$ is concave. The second law of thermodynamics then states that this entropy must increase along streamlines: $d\eta \geq 0$, so that the mixture tends towards the mixture defined by the equilibrium state of the previous section. In order to define the evolution of $M_1/M$ and $E_i/E$ towards $\overline{M}_1/M$ and $\overline{E}_i/E$, the terms $d(M_1/M)$ and $d(E_i/E)$ of equation (16) have to be modeled in agreement with the increase of the mixture entropy, $d\eta \geq 0$. For the sake of readability, we set:

$$\mathcal{Y} = \left(\frac{M_1}{M}, \frac{M_2}{M}, \frac{M_3}{M}, \frac{M_4}{M}, \frac{E_1}{E}, \frac{E_1}{E}, \frac{E_1}{E}, \frac{E_1}{E}\right),$$

and $\overline{\mathcal{Y}}$ its equilibrium counterpart.

We choose here a classical BGK modeling approach and we set:

$$d\left(\frac{M_i}{M}\right) = \frac{\overline{M}_i - M_i}{M\ \lambda},\ i = 1..4, \quad \text{and} \quad d\left(\frac{E_i}{E}\right) = \frac{\overline{E}_i - E_i}{E\ \lambda},\ i = 1..4, \tag{25}$$

where $\lambda$ is a positive time-scale. It can be proved that these source terms lead to an increase of the entropy. Indeed, the Gibbs relation (15) can also be written:

$$d\eta = \sum_{i=1}^{4} \frac{\partial \eta}{\partial (E_i/E)}_{|\mathcal{Y}\backslash(E_i/E)} d\left(\frac{E_i}{E}\right) + \sum_{i=1}^{4} \frac{\partial \eta}{\partial (M_i/M)}_{|\mathcal{Y}\backslash(M_i/M)} d\left(\frac{M_i}{M}\right). \tag{26}$$

In relation (26), the notation $\mathcal{Y}\backslash(E_i/E)$ (respectively $\mathcal{Y}\backslash(M_i/M)$) means that the partial derivatives is computed with all the components of the vector $\mathcal{Y}$ fixed except the one associated with $E_i/E$ (respectively $M_i/M$). Since the mixture entropy is concave with respect to $\mathcal{Y}$ (see section 2.1.3), the tangent plane to $\eta$ is always above $\eta$, in particular when considering the equilibrium state we have:

$$\forall \mathcal{Y}, \qquad \eta(\overline{\mathcal{Y}}) \leq \eta(\mathcal{Y}) + \sum_{i=1}^{4} \frac{\partial \eta}{\partial (E_i/E)}_{|\mathcal{Y}\backslash(E_i/E)} \left(\overline{E}_1 - E_1\right) + \sum_{i=1}^{4} \frac{\partial \eta}{\partial (M_i/M)}_{|\mathcal{Y}\backslash(M_i/M)} \left(\overline{M}_i - M_i\right).$$

The equilibrium state $\overline{\mathcal{Y}}$ corresponds to the maximum of $\eta$, so that we have $\eta(\overline{\mathcal{Y}}) - \eta(\mathcal{Y}) \geq 0$ and thus we get:

$$\forall \mathcal{Y}, \qquad 0 \leq \sum_{i=1}^{4} \frac{\partial \eta}{\partial (E_i/E)}_{|\mathcal{Y}\backslash(E_i/E)} \left(\overline{E}_1 - E_1\right) + \sum_{i=1}^{4} \frac{\partial \eta}{\partial (M_i/M)}_{|\mathcal{Y}\backslash(M_i/M)} \left(\overline{M}_i - M_i\right). \tag{27}$$

The time-scale $\lambda$ is positive, hence by introducing source terms (25) into the Gibbs relation (26) and using the inequality (27), we straightforwardly obtain that $d\eta \geq 0$. As a consequence, the BGK source terms defined by (25) are in agreement with the second law of thermodynamics provided that $\lambda > 0$.

Source terms (25) share the same time-scale $\lambda$. This is a key point in the proof above. In a physical point of view, this means that the return towards the equilibrium is the same for temperatures and for the masses. This choice has been retained here but other possibilities exist for modeling the source terms. Modified BGK source terms have been proposed in [24] for two-phase steam-liquid flows. They allow to define different and independent time scales (for instance one for the thermal disequilibrium and an other one for the chemical reaction), though they may lead to more complex numerical schemes when turning to simulations. One could also choose independent source terms on the basis of the entropy gradient, as often used for multi-velocity models, but once again the associated numerical scheme can become complex. It will be seen in section 3.3 that building numerical scheme for discretizing source terms (25) is a simple task.

**Remark.** *It should be noted that $\lambda$ represents the inverse of the reaction rate.*

**Remark.** *When the chemical reaction is not possible, sole the thermal disequilibrium has to be accounted for (see section 2.1.3). In Gibbs relation* (16) *we have thus $d(M_i/M) = 0$ for $i = 1..4$ and it reduces to:*

$$d\eta = E \sum_{i=1}^{3} \left(\frac{1}{T_i} - \frac{1}{T_4}\right) d\left(\frac{E_i}{E}\right). \tag{28}$$

*It should be noted that since the entropy $\eta$ is strictly concave with respect to $(M_i/M, E_i/E)_{i=1..4}$, then it is also strictly concave with respect to $(E_i/E)_{i=1..4}$ (for fixed $(M_i/M)_{i=1..4}$). Hence, the source terms defined in the present section are still in agreement with the second law of thermodynamics when only accounting for the relaxation to the thermal equilibrium without chemical reaction.*

### 2.1.5 The convective model in intensive form

In this section, a complete set of partial derivative equations is built on the basis of the previous sections. This set of equations is based on the Euler model in intensive formulation and in one-dimensional domain. It is then straightforward to extend the model to three-dimensional domains , see section 3. The thermal diffusion terms are accounted for afterwards in section 2.1.6 and the final model is then based on the compressible Navier-Stokes model. Diffusion effects have been treated separately in order to highlight the specificity of the assumptions that each gas possesses its own temperature.

We first assume that all the gases share the same velocity field $U$, so that all the derivative operators of the previous sections can be seen as derivatives along the streamlines:

$$d\phi \longleftrightarrow \partial_t(\phi) + U\partial_t(\phi).$$

Moreover, it is also assumed that:

- the mass of the mixture $M$ is constant along the streamlines : $dM = 0$;
- the evolution of the volume of the mixture is linked to the divergence of the velocity field, which reads in the one-dimensional setting: $dV/V = \partial_x(U)$;
- the Newton's law is applied to the mixture by only considering the force due to the mixture pressure, it reads in the one-dimensional setting: $MdU = \partial_x(P)$;
- the first law of thermodynamics is applied to the energy of the mixture in agreement with the Newton's law above: $dE = -PdV$

We thus obtain the following set of equations in an extensive form:

$$\begin{cases} d\left(\frac{M_i}{M}\right) = \frac{\overline{M}_i - M_i}{M\ \lambda},\ i = 1..3, \\ d\left(\frac{E_i}{E}\right) = \frac{\overline{E}_i - E_i}{E\ \lambda},\ i = 1..3, \\ dM = 0, \\ dV/V = \partial_x(U), \\ MdU = \partial_x(P), \\ dE = -PdV. \end{cases} \tag{29}$$

System (29) can then be translated in terms of intensive variables by dividing by the mass $M$ which is constant. The system of equations in intensive form then reads:

$$\begin{cases} \partial_t(\rho Y) + \partial_x(\rho U Y) = \rho\frac{\overline{Y} - Y}{\lambda}, \\ \partial_t(\rho) + \partial_x(\rho U) = 0, \\ \partial_t(\rho U) + \partial_x\left(\rho U^2 + P\right) = 0, \\ \partial_t(\rho\mathcal{E}) + \partial_x(U(\rho\mathcal{E} + P)) = 0, \end{cases} \tag{30}$$

where $\rho = M/V = \sum_{i=1}^4 M_i/V$ is the density, $\tau = 1/\rho$ is the specific volume, $P$ is the mixture pressure defined in section (2.1.1), $\mathcal{E} = e + U^2/2$ is the specific total energy and $e = E/M = \sum_{i=1}^4 E_i/M$ is the specific internal energy. The two vectors $Y$ and $\overline{Y}$ gather respectively the fractions defining the mixture and the fractions defining the equilibrium state: $Y = (y_1, y_2, y_4, z_1, z_2, z_4)$ and $\overline{Y} = (\overline{y}_1, \overline{y}_2, \overline{y}_4, \overline{z}_1, \overline{z}_2, \overline{z}_4)$. The mass fraction $y_i$ of gas $i$ is $y_i = M_i/M$ and the energy fraction $z_i$ of gas $i$ reads $z_i = E_i/E$. It should be noted that the mass fraction and the energy fraction of gas 3 are not computed, but they can be deduced from $Y$ according to the relations: $y_3 = 1 - (y_1 + y_2 + y_4)$ and $z_3 = 1 - (z_1 + z_2 + z_4)$. With these definitions, one can express the specific volume $\tau_i$ of gas $i$ as:

$$\tau_i = \frac{V_i}{M_i} = \frac{V}{M_i} = \frac{V}{M}\frac{M}{M_i} = \frac{\tau}{y_i}, \tag{31}$$

and the specific energy of gas $i$ as:

$$e_i = \frac{E_i}{M_i} = \frac{E}{M}\frac{E_i}{E}\frac{M}{M_i} = \frac{z_i e}{y_i}. \tag{32}$$

The mixture density and the mixture internal energy are then: $\rho = \sum_{i=1}^4 \rho_i$, with $\rho_i = 1/\tau_i$, and $e = \sum_{i=1}^4 y_i e_i$. Hence, system of equations (30) possesses nine equations and the nine primitive intensive unknowns are: $Y$, $\tau$ (or $\rho$), $U$ and $e$. All the other quantities, including the pressures, the temperature and the equilibrium state $\overline{Y}$ can be expressed with respect to these nine unknowns. In particular, the mixture pressure and the mixture temperature are:

$$\frac{P(Y,\tau,e)}{T(Y,\tau,e)} = \sum_{i=1}^4 \frac{P_i\left(\frac{\tau}{y_i}, \frac{z_i e}{y_i}\right)}{T_i\left(\frac{\tau}{y_i}, \frac{z_i e}{y_i}\right)} \quad \text{and} \quad \frac{1}{T(Y,\tau,e)} = \sum_{i=1}^4 \frac{z_i}{T_i\left(\frac{\tau}{y_i}, \frac{z_i e}{y_i}\right)}.$$

The pressure and temperature of gas $i$ are obtained from the specific entropy $s_i = \eta_i/M_i$. The entropy of each gas $i$ is PH1 (see section (2.1.1)), therefore for $M_i > 0$ we have (with an abuse of notation):

$$\frac{\eta_i(V, M_i, E_i)}{M_i} = \eta_i\left(\frac{V}{M_i}, \frac{M_i}{M_i}, \frac{E_i}{M_i}\right) = \eta_i(\tau, y_i, z_i e) = s_i\left(\frac{\tau}{y_i}, \frac{z_i e}{y_i}\right).$$

The definition of the temperature and pressure of gas $i$ given in section (2.1.1) can be written on the basis of the intensive quantities by using the fact that $M_i$ is constant in these definitions:

$$\frac{P_i}{T_i} = \frac{\partial \eta_i}{\partial V_i}_{|M_i,E_i} = \frac{\partial(\eta_i/M_i)}{\partial(V_i/M_i)}_{|E_i/M_i} = \frac{\partial s_i}{\partial \tau_i}_{|e_i}$$

and

$$\frac{1}{T_i} = \frac{\partial \eta_i}{\partial E_i}_{|M_i,V_i} = \frac{\partial(\eta_i/M_i)}{\partial(E_i/M_i)}_{|V_i/M_i} = \frac{\partial s_i}{\partial e_i}_{|\tau_i}$$

It should be added that the specific mixture entropy is $s = \eta/M = \sum_{i=1}^{4} y_i s_i$. The model in intensive form proposed here and composed of the system of equations (30) and of the closures described above accounts for the convective effects and for the return to the equilibrium issued from the thermo-chemistry of the combustion of hydrogen. Let us now introduce the effect of the thermal diffusion in system (30).

### 2.1.6 Accounting for the thermal diffusion into the gases

System of equations (30) only account for the convective effects and for the chemical reaction. In order to simulate the propagation of the combustion flame, it is mandatory to also take into account the thermal diffusivity. Indeed, in a physical point of view the propagation of the combustion front is the result of the combination of the chemical reaction and the diffusion of the temperature into the gases. The chemical reaction induces an increase of the temperature in the burnt gases. Near the flame front, the thermal diffusion transfers heat from the burnt gases to the neighboring unburnt gases. This implies an increase of the temperature in the unburnt gases and this then activates the chemical reaction in the unburnt gases. Therefore, the front between burnt and unburnt gases propagates into the unburnt gases.

The energy fractions $z_i$ of each gas are variables of model (30), and this allows to account for the thermal diffusion within each gas. First, the equation for the mixture internal energy, $e = \mathcal{E} - U^2/2$ can be obtained by combining the equation of the total energy and the momentum equation of system (30). It reads:

$$\partial_t(\rho e) + \partial_x(\rho e U) + P\partial_x(U)) = 0. \tag{33}$$

The combination of definitions (31) and (32) gives that: $\rho_i e_i = z_i \times (\rho e)$, which leads to:

$$\partial_t(\rho_i e_i) + \partial_x(\rho_i e_i U) = z_i(\partial_t(\rho e) + \partial_x(\rho e U)) + \rho e(\partial_t(z_i) + U\partial_x(z_i)) \tag{34}$$

Then, by using the derivative equation (33) and the derivative equation for $z_i$, we get a derivative equation for $(\rho_i e_i)$, the internal energy (per unit of volume) of each gas:

$$\partial_t(\rho_i e_i) + \partial_x(\rho_i e_i U) + z_i P\partial_x(U) = \rho e\left(\frac{\overline{z}_i - z_i}{\lambda}\right). \tag{35}$$

The thermal diffusion is added to the model by adding a diffusion operator on equations (35), they thus now reads:

$$\partial_t(\rho_i e_i) + \partial_x(\rho_i e_i U) + z_i P\partial_x(U) = \partial_x(D_i\partial_x(T_i)) + \rho e\left(\frac{\overline{z}_i - z_i}{\lambda}\right), \tag{36}$$

where $D_i \geq 0$ is the thermal diffusion coefficient for gas $i$ (in $W/m/K$). Since we have $\rho e = \sum_{i=1}^{4} \rho_i e_i$, $\sum_{i=1}^{4} z_i = 1$ and $\sum_{i=1}^{4} \overline{z}_i = 1$, the new derivative equation for $\rho e$ is obtained by summing (36) over the gases $i$ and it yields:

$$\partial_t(\rho e) + \partial_x(\rho e U) + P\partial_x(U) = \sum_{i=1}^{4} \partial_x(D_i\partial_x(T_i)). \tag{37}$$

It should be noted that the modification of equation (35) into equation (36) also modifies the derivative equation for $z_i = \rho_i e_i/(\rho e)$. Indeed, by combining equations (37) and (36) we obtain:

$$\partial_t(z_i) + U\partial_x(z_i) = \frac{\partial_x(D_i\partial_x(T_i)) - z_i\sum_{j=1}^{4}\partial_x(D_j\partial_x(T_j))}{\rho e} + \left(\frac{\overline{z}_i - z_i}{\lambda}\right). \tag{38}$$

Finally, in order to account for the thermal diffusion of the gases, system (30) is modified into:

$$\begin{cases} \partial_t(\rho y_i) + \partial_x(\rho U y_i) = \rho\frac{\overline{y}_i - y_i}{\lambda}, \quad i = 1..3, \\ \partial_t(\rho z_i) + \partial_x(\rho U z_i) = \rho\frac{\overline{z}_i - z_i}{\lambda} + \frac{1}{e}\left(\partial_x(D_i\partial_x(T_i)) - z_i\mathcal{D}\right), \quad i = 1..3, \\ \partial_t(\rho) + \partial_x(\rho U) = 0, \\ \partial_t(\rho U) + \partial_x\left(\rho U^2 + P\right) = 0, \\ \partial_t(\rho\mathcal{E}) + \partial_x(U(\rho\mathcal{E} + P)) = \mathcal{D}, \end{cases} \tag{39}$$

where we have set $\mathcal{D} = \sum_{i=1}^{4} \partial_x \left( D_i \partial_x \left( T_i \right) \right)$ to denote the diffusion operator for the mixture energy.

**Remark.** *It is an important point to be quoted that in a numerical point of view, equations* (36) *will be preferred for accounting for the thermal fluxes instead of equations* (38) *and* (37)*. The former are indeed far more convenient for ensuring energy conservation and for maintaining the discrete maximum principle for* $z_i$*. This point is detailed in section 3.2.*

### 2.1.7 Summary of the main assumptions of the model

Here is a short summary of the main assumptions that have been made all along section 2 for building the model.

- We consider a mixture of 4 miscible gases.
- Each gas possesses its own pressure, its own temperature and its own thermal diffusivity.
- We account for a simple one-step reaction.
- The reaction rate is given by an Arrhenius law based on the mixture temperature.
- Turbulence and molecular viscosity are not taken into account.

The model can thus deal with a lot of industrial large-scale configurations where a one-step reaction is sufficient to describe $H_2$ combustion. Its main weakness is that it does not account for turbulence, which is essential for industrial simulations. This point is clearly the main objective of ongoing work.

## 2.2 Properties of the model

In the present section, we focus on some properties of system of equations (39) which has been written in conservative form in the previous sections. Most of them are directly inherited from the Navier-Stokes system of equations which forms the basis of the model. More details on the different mathematical definitions can be found for instance in [17, 40].

### 2.2.1 Hyperbolicity and eigen-structure

We only consider here the terms involving first order derivatives in time and space. System (39) then reduces to the Euler system of equations supplemented by advection equations of the mass and energy fractions. In addition, the pressure-law is the complex non-linear mixture pressure-law $(Y, \tau, e) \mapsto P(Y, \tau, e)$:

$$\left\{ \begin{array}{l} \partial_t \left( \rho Y \right) + \partial_x \left( \rho U Y \right) = 0, \\ \partial_t \left( \rho \right) + \partial_x \left( \rho U \right) = 0, \\ \partial_t \left( \rho U \right) + \partial_x \left( \rho U^2 + P(Y, \tau, e) \right) \big) = 0, \\ \partial_t \left( \rho \mathcal{E} \right) + \partial_x \left( U(\rho \mathcal{E} + P(Y, \tau, e)) \right) = 0, \end{array} \right. \tag{40}$$

Let us define the variable $Z = (Y, s, U, P)$. The Jacobian matrix $A(Z)$ of system (40) can easily been expressed using $Z$ and it reads in compact form:

$$A(Z) = \left( \begin{array}{c|ccc} U \times \mathcal{I}_6 & \multicolumn{3}{c}{\underline{\mathbf{0}}_{6,3}} \\ \hline & U & 0 & 0 \\ \underline{\mathbf{0}}_{3,6} & 0 & U & \tau \\ & 0 & \frac{C^2}{\tau} & U \end{array} \right), \tag{41}$$

where $\mathcal{I}_6$ is the $6 \times 6$ identity matrix, $\underline{\mathbf{0}}_{k,l}$ represents the zero matrix with $k$ lines and $l$ columns, and where $C$ denotes the speed of sound in the mixture defined by:

$$C^2 = \tau^2 \left( P \frac{\partial P}{\partial e}_{|Y,\tau} - \frac{\partial P}{\partial \tau}_{|Y,e} \right). \tag{42}$$

The square of the speed of sound $C^2$ can also be rewritten with respect to the specific entropies $s_i$ thanks to the definition of the pressure $P$ and of the temperature $T$:

$$-\frac{C^2}{T\tau^2} = \sum_{i=1}^{4} \frac{1}{y_i} (-1, z_i P) \cdot s_i'' \cdot (-1, z_i P)^\top, \quad \text{with} \quad s_i'' = \left( \begin{array}{cc} \frac{\partial^2 s_i}{\partial \tau_i^2} & \frac{\partial^2 s_i}{\partial \tau_i \partial e_i} \\ \frac{\partial^2 s_i}{\partial \tau_i \partial e_i} & \frac{\partial^2 s_i}{\partial e_i^2} \end{array} \right). \tag{43}$$

We recall that each specific entropy $s_i$ is strictly concave, see section 2.1.1. Hence, provided that $T$ is positive, relation (43) ensures that $C^2$ is positive and thus that $C$ is correctly defined in $\mathbb{R}^+$ through (42). The eigenvalues $\lambda_i$, $i = 1..9$, and the associated right eigenvectors $V_i$, $i = 1..9$, of Jacobian matrix (41) can easily be obtained and they read:

$$\lambda_j = U, \quad V_j = (\delta_{(i,j)})_i, \quad j = 1..6, \tag{44}$$

$$\lambda_7 = U - C, \quad V_7 = (\underline{\mathbf{0}}_{1,6}, 0, 1, -C/\tau), \tag{45}$$

$$\lambda_8 = U, \quad V_8 = (\underline{\mathbf{0}}_{1,6}, 1, 0, 0), \tag{46}$$

$$\lambda_9 = U + C, \quad V_9 = (\underline{\mathbf{0}}_{1,6}, 0, 1, C/\tau), \tag{47}$$

where $\delta_{(i,j)} = 1$ if $i = j$ and 0 otherwise. The first six eigenvectors $V_i$, $i = 1..6$, are the first six vectors of the canonical basis. Therefore, provided that $C \neq 0$, the nine right eigenvectors span the whole space $\mathbb{R}^9$. **As a consequence, system** (40) **is hyperbolic provided that** $C \neq 0$.

The fields associated with $\lambda_7$ and $\lambda_9$ are genuinely non-linear while the eight other fields are linearly degenerate. The system is then composed of three waves: a $U - C$ shock or rarefaction wave, a $U$ contact wave and a $U + C$ shock or rarefaction wave. The Riemann invariants in the $U \pm C$ rarefaction waves are:

$$Y, \quad s \quad \text{and} \quad \left( U \mp \int_{P_0}^{P} \frac{\tau(Y,s,p)}{C(Y,s,p)} dp \right),$$

and the Riemann invariants in the contact-wave are: $U$ and $P$. An important point to be quoted is that the fractions are constants across the rarefaction waves. The shock waves are studied in the next section.

### 2.2.2 Shock waves and the Rankine-Hugoniot relations

When focusing on the convective part of model (40), the jump conditions in a shock wave traveling with a speed $\sigma$ are given by the classical Rankine-Hugoniot relations. Let us denote by a subscript + (resp. −) the state on the left (resp. right) of the discontinuity, and let us note for any quantity $\phi$: $[\phi] = \phi^+ - \phi^-$ and $\widetilde{\phi} = (\phi^+ + \phi^-)/2$. The Rankine-Hugoniot jump relations for system (40) are then:

$$\begin{cases} -\sigma[\rho Y] + [\rho U Y] = 0, \\ -\sigma[\rho] + [\rho U] = 0, \\ -\sigma[\rho U] + [\rho U^2 + P] = 0, \\ -\sigma[\rho \mathcal{E}] + [U(\rho \mathcal{E} + P)] = 0. \end{cases} \tag{48}$$

The mass flux across the shock is $J = \rho(U - \sigma)$ and the mass equation in (48) leads to $[J] = 0$. Since $\sigma$ is a constant, it also leads to $J[\tau] = [U]$. If vacuum does not occurs, the sound speed is strictly positive and the eigenvalues of the system are ordered: $U - C < U < U + C$. As a consequence, we get that in a shock wave $\sigma \neq U$ or equivalently that $J \neq 0$. System (48) can then be simplified in:

$$\begin{cases} [J] = 0, \\ J[Y] = 0, \\ J[U] + [P] = 0, \\ J[\mathcal{E}] + [UP] = 0, \end{cases} \iff \begin{cases} J[\tau] = [U], \\ [Y] = 0, \\ J^2[\tau] + [P] = 0, \\ [e] + \widetilde{P}[\tau] = 0. \end{cases} \tag{49}$$

The third equation of (49) is called the Rayleigh line (it represents a line in the $(\tau^+, P^+)$ plane when $(\tau^-, P^-)$ and $J$ are fixed) and the forth one is called the Hugoniot curve. It should be noted that the fractions do not change across a shock wave $[Y] = 0$. Therefore, the second property $(ii)$ of proposition 2.3 allows to correctly define the shocks by ensuring the uniqueness of the solution of the Rankine-Hugoniot relations. Indeed, by combining first and third equations of (49) we obtain: $[U]^2 = -[\tau][P]$, which does not allow to define $[U]$ in a unique manner. With the help of the concavity property $(ii)$ of proposition 2.3, it can be shown that a shock wave is admissible - in the sense that it leads to an increase of the entropy - if and only if $[U] < 0$ (see [17, 13]). We thus get the following set of jump relations for admissible shock waves:

$$\begin{cases} \sigma = [\rho U]/[\rho], \\ [Y] = 0, \\ [U] = -\sqrt{-[\tau][P]}, \\ [e] + \widetilde{P}[\tau] = 0. \end{cases} \tag{50}$$

We focus now on system (30) - which corresponds to system (39) where the thermal diffusion is neglected - but where the relaxation time scale $\lambda$ tends to zero. This corresponds to the case of an instantaneous chemical

reaction: $Y = \overline{Y}$. Formally the pressure law thus becomes: $(\tau, e) \mapsto \overline{P}(\tau, e) = P(\overline{Y}(Y_0, \tau, e), \tau, e))$, where $Y_0$ stands for the initial fractions that are used for initializing the mixture before the reaction occurs. We consider a discontinuity in the solution that travels at speed $\sigma$ and that separates two states with subscript $+$ and $-$. For this degenerate case, the fraction $Y$ are no more variables and the corresponding jump relation in system (50) does not hold anymore. The Rankine-Hugoniot relations between these to states are then:

$$\begin{cases} \sigma = [\rho U]/[\rho], \\ [U] = -\widetilde{\sqrt{-[\tau][\overline{P}]}}, \\ [e] + \widetilde{(\overline{P})}[\tau] = 0. \end{cases} \tag{51}$$

This system of relations is often studied in a simplified form (in particular regarding the EOS) for determining in an analytical manner the jump of the physical quantities across thin flame front. Different regimes of the shock waves are then studied: strong or weak deflagration, strong of weak detonation, even if all these regimes are not encountered in combustion waves [43].

### 2.2.3 Thermal diffusion and entropy inequality

In this section, we focus on the contribution of the thermal diffusion to the entropy balance for the mixture. System (39) is considered but source terms are not accounted for. For regular solutions, it thus respectively leads to the equations for the fractions, for the specific volume of the mixture and for the mixture internal energy:

$$\partial_t (y_i) + U\partial_x (y_i) = 0, \quad i = 1..3, \tag{52}$$

$$\partial_t (z_i) + U\partial_x (z_i) = \frac{1}{\rho e}(\partial_x (D_i \partial_x (T_i)) - z_i \mathcal{D}), \quad i = 1..3, \tag{53}$$

$$\partial_t (\tau) + U\partial_x (\tau) = \tau \partial_x (U), \tag{54}$$

$$\partial_t (e) + U\partial_x (e) = \tau \mathcal{D} - \tau P \partial_x (U). \tag{55}$$

The equation for the specific mixture entropy $(Y, \tau, e) \mapsto s(Y, \tau, e)$ reads:

$$\partial_t (s) + U\partial_x (s) = e \sum_{i=1}^{4} (\partial_t (z_i) + U\partial_x (z_i)) + \frac{P}{T} (\partial_t (\tau) + U\partial_x (\tau)) + \frac{1}{T} (\partial_t (e) + U\partial_x (e)),$$

which by using equations (52), (53), (54) and (55) gives:

$$\partial_t (s) + U\partial_x (s) = \tau \sum_{i=1}^{4} \left( \frac{\partial_x (D_i \partial_x (T_i))}{T_i} \right). \tag{56}$$

Let us now consider a volume of fluid $\Omega$ which is isolated from its surroundings in the sense that the thermal fluxes associated with the thermal diffusion are equal to zero on the boundary $\partial\Omega$ of $\Omega$: $(\lambda_i \partial_x (T_i).n)(w),\ i = 1..4$, for all $w \in \partial\Omega$, where $n$ is the unit normal to $\partial\Omega$ . Then the integral of equation (56) over $\Omega$ is:

$$\int_\Omega \rho (\partial_t (s) + U\partial_x (s))\ dx = \sum_{i=1}^{4} \int_\Omega \left( \frac{\partial_x (D_i \partial_x (T_i))}{T_i} \right)\ dx,$$

$$\int_\Omega \rho (\partial_t (s) + U\partial_x (s))\ dx = \sum_{i=1}^{4} \left( -\int_{\partial\Omega} \left( \frac{D_i}{T_i} \partial_x (1/T_i) \right).n\ dw + \int_\Omega \left( D_i T_i^2 (\partial_x (1/T_i))^2 \right)\ dx \right)$$

Since the heat fluxes are null for each gas on $\partial\Omega$, we get:

$$\int_\Omega \rho (\partial_t (s) + U\partial_x (s))\ dx = \sum_{i=1}^{4} \int_\Omega \left( D_i T_i^2 (\partial_x (1/T_i))^2 \right)\ dx. \tag{57}$$

Since $D_i \geq 0$, each integral in the sum on the right hand side of equation (57) is positive, so that we can conclude that for all set $\Omega$ such that $(\lambda_i \partial_x (T_i).n)(w) = 0,\ i = 1..4$, for all $w \in \partial\Omega$:

$$\int_\Omega \rho (\partial_t (s) + U\partial_x (s))\ dx \geq 0, \tag{58}$$

or by using the (mixture) mass equation, i.e. the third equation of system (39):

$$\int_\Omega (\partial_t (\rho s) + \partial_x (\rho U s))\ dx \geq 0, \tag{59}$$

In the sense of equation (58) or (59), the diffusion operator is in agreement with the second law of thermodynamics and thus with the source terms that rule the chemical reaction and the thermal equilibrium (see section 2.1.4).

### 2.2.4 Maximum principle for the fractions

Each mass fraction obeys a convection equation with a source term, while the equations for the energy fractions involve an additional diffusion operator that arises from the thermal diffusion. The convective part of these equations allows to maintain the fraction in $[0,1]$ provided that they initially belong to $[0,1]$ and that the fractions at the inlet boundaries (where the entering mass flow rate is positive) is in $[0,1]$.

Concerning the source terms, they all have been written in a BGK form: $(\overline{Y}-Y)/\lambda$, with $\lambda>0$, and where the equilibrium fractions $\overline{Y}$ defined in section 2.1.3 belongs to $[0,1]$ provided that for all $i$: $\overline{M}_i \geq 0$ and $\overline{E}_i \geq 0$. It is an important point to be noted here that, if the condition $\overline{M}_i \geq 0$ is natural, the second one may not be fulfilled. Indeed, when considering for instance Stiffened Gas EOS (or even the Chemkin EOS, which is a Stiffened Gas EOS with a calorific capacity that depends on the temperature), the internal energy is: $e_i = Q_i + C_{v,i}T_i$, where thanks to the properties of the specific entropies we have $T_i > 0$ (see section 2.1.1). The parameter $Q_i$ is an activation energy which may be negative. As a consequence, for small enough temperature $e_i$ may become negative, leading to energy fractions that may not belong to $[0,1]$. Moreover, this feature can also implies a loss of hyperbolicity by giving a negative mixture temperature (which is the combination of the temperature $T_i > 0$ weighted by the energy fractions). Thus through definition (43), the square of the sound speed $C^2$ can be negative even for strictly concave phasic entropies.

It then remains to treat the diffusion term in the equations for the energy fractions. Let us write this equation without the convective terms and without the source terms:

$$\rho e \partial_t\left(z_i\right) = \partial_x\left(D_i \partial_x\left(T_i\right)\right) - z_i \mathcal{D}, \quad i = 1..4, \tag{60}$$

or using the energy formulation (36) of section 2.1.6:

$$\partial_t\left(\rho_i e_i\right) = \partial_x\left(D_i \partial_x\left(T_i\right)\right), \quad i = 1..4. \tag{61}$$

Indeed, it should be recalled that we have:

$$z_i = \frac{(\rho_i e_i)}{\sum_{j=1}^{4}(\rho_j e_j)}. \tag{62}$$

Let us integrate equation (61) over a volume of fluid $\Omega$, we get:

$$\int_\Omega \partial_t\left(\rho_i e_i\right)\ dx = \int_{\partial\Omega} \left(D_i \partial_x\left(T_i\right).n\right)(w)\ dw, \quad i = 1..4. \tag{63}$$

If the thermal flux $\left(D_i \partial_x\left(T_i\right).n\right)$ tends to zero when $\rho_i e_i(x)$ tends to zero for all $x$ in $\Omega$, we are ensured that the integral on the left hand side of equation (63) also tends to zero. In other words, if the thermal flux vanishes at the boundary $\partial\Omega$ when the energy of the volume $\Omega$ tends to zero, then the energy $(\rho_i e_i)$ in $\Omega$ remains positive. Obviously, this property strongly relies on the property of the chosen EOS. For instance, it may not hold for Stiffened Gas EOS, as already explained in the previous paragraph. Nevertheless, when this property holds, the positivity of $\rho_i e_i$ ensures that $z_i$ belongs to $[0,1]$ thanks to definition (62).

**Remark.** *The numerical scheme for the thermal fluxes is detailed in section 3.2. It is based on the previous point, and on equations* (62) *and* (63).

# 3 Description of the numerical schemes

The aim of the present section is to describe the numerical strategy that has been retained in order to compute approximated solutions of the model of section 2. We first write the three-dimensional counterpart of system of equations (39):

$$\left\{\begin{array}{l} \partial_t\left(\rho y_i\right) + \nabla\cdot\left(\rho U y_i\right) = \rho\frac{\overline{y}_i - y_i}{\lambda}, \quad i = 1..3, \\ \partial_t\left(\rho z_i\right) + \nabla\cdot\left(\rho U z_i\right) = \rho\frac{\overline{z}_i - z_i}{\lambda} + \frac{1}{e}(\nabla\cdot\left(D_i\nabla\left(T_i\right)\right) - z_i\mathcal{D}), \quad i = 1..3, \\ \partial_t\left(\rho\right) + \nabla\cdot\left(\rho U\right) = 0, \\ \partial_t\left(\rho U\right) + \nabla\cdot\left(\rho U\otimes U + P\times\mathcal{I}_3\right) = 0, \\ \partial_t\left(\rho\mathcal{E}\right) + \nabla\cdot\left(U(\rho\mathcal{E}+P)\right)x = \mathcal{D}, \end{array}\right. \tag{64}$$

where $U = (U_x, U_y, U_z)$ now denotes the velocity vector, $\mathcal{E} = U\cdot U/2 + e$ is the specific total energy, and where the thermal diffusivity term now reads $\mathcal{D} = \sum_{i=1}^{4}\nabla\cdot\left(D_i\nabla\left(T_i\right)\right)$. In system (64), operators $\nabla\cdot()$ and $\nabla()$ respectively denote the divergence in space and the gradient in space. System of equations (64) involves different

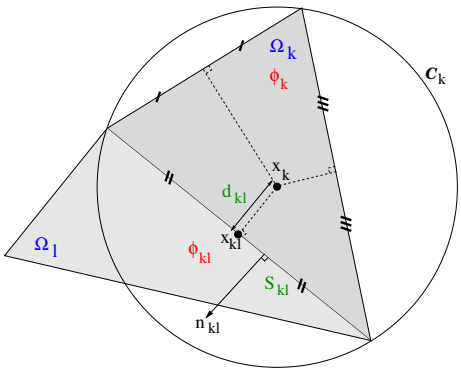


Figure 1: Notation for a given triangular cell $k$ (and one of its neighbor $l$) of the mesh and for a given quantity $\Phi$.

operators: first order derivative terms, source terms and second order derivative operators. The overall strategy applied in the present section relies on a Finite Volumes discretization and on a fractional step algorithm in time (a Lie-Trotter splitting). At each time-step, first- and second-order derivative terms are first treated and source terms are accounted for afterwards. The convective and diffusion fluxes are computed through first-order explicit schemes respectively described in section 3.1 and 3.2. The time step is computed on the basis of the CFL constraint for the sole convective terms. The latter may thus be not well-suited for small mesh sizes, for which explicit diffusion fluxes lead to unstable approximations (the Fourier constraint is more restrictive than the CFL constraint for small mesh sizes). This point is directly linked with the classical technique of *artificial thickening of the flame* which is presented in details in section 4.2. At last, the source terms are treated semi-implicitly in order to overcome their stiffness (which is related to the time scale $\lambda$), see section 3.3.

At last, let us introduce some classical notations used to describe the Finite Volumes discretization on a mesh. We restrict here to triangular meshes in 2D and to tetrahedral meshes in 3D. These restrictions are made for two reasons:

- spurious modes due to the inaccuracy of first order explicit scheme for the computation of the convective fluxes for low-Mach flows can be avoided with such cells (see also section 3.1);
- first order diffusive fluxes can be written in a consistent manner on these kind of cells by using the center of the circumcircle (or circumsphere in 3D) of the cells (see section 3.2)[2].

The sketch of the notations for the 2D case can be found in figure 1 for a triangular cell $\Omega_k$. The triangular cell $\Omega_k$ has a volume $|\Omega_k|$ and the center of its circumscribed circle $\mathcal{C}_k$ is $x_k$. [3] Considering a neighbor $l$ of cell $\Omega_k$, subscripts $kl$ refer to the properties associated with these two cells: $S_{kl}$ denotes the measure of the surface of the face that separates the two cells, $n_{kl}$ is the unit normal to the common face oriented from $\Omega_k$ to $\Omega_l$ (with $n_{kl} = -n_{lk}$) and $x_{kl}$ stands for the barycenter of the face $kl$ (with $x_{kl} = x_{lk}$). The distance between $x_k$ and $x_{kl}$ is denoted by $d_{kl} = |x_k - x_{kl}|$ with in general $d_{kl} \neq d_{lk}$. We consider Finite Volume schemes so that in a cell $\Omega_k$, any quantity $\Phi(t, x)$ is approximated by $\Phi_k(t)$ which is defined as the spatial-average of $\Phi$ over $\Omega_k$ at time $t$:

$$\Phi_k(t) = \frac{1}{|\Omega_k|} \int_{\Omega_k} \Phi(t, x) dx.$$

Moreover, in order to discretize the time derivatives, we introduce the notation $\Phi_k^n = \Phi_k(t^n)$ which corresponds to the value of $\Phi_k$ at time $t^n$.

## 3.1 Discretization of the convective terms

The convective part of system (64) is:

$$\left\{ \begin{array}{l} \partial_t(\rho y_i) + \nabla \cdot (\rho U y_i) = 0, \quad i = 1..3, \\ \partial_t(\rho z_i) + \nabla \cdot (\rho U z_i) = 0, \quad i = 1..3, \\ \partial_t(\rho) + \nabla \cdot (\rho U) = 0, \\ \partial_t(\rho U) + \nabla \cdot (\rho U \otimes U + P \times \mathcal{I}_3) = 0, \\ \partial_t(\rho \mathcal{E}) + \nabla \cdot (U(\rho \mathcal{E} + P))\, x = 0, \end{array} \right. \tag{65}$$

[2] For that point, Voronoï type cells would lead to the same consistency of the diffusive fluxes.

[3] It should be noted that for triangles with one angle with a measure greater than $\Pi/2$, $x_k$ may be located outside $\Omega_k$ ; and for right-angled triangle $\Omega_k$ with $kl$ being the hypothenuse, we have $x_k = x_{kl}$.

or using a compact form:

$$\partial_t(\mathcal{W}) + \nabla \cdot (\mathcal{F}(\mathcal{W})) = 0,$$

where, by using an abuse of notation considering the fraction vector $Y$ and the velocity vector, we have:

$$\mathcal{W} = (\rho Y, \rho, \rho U, \rho \mathcal{E}) \quad \text{and} \quad \mathcal{F}(\mathcal{W}) = (\rho U Y, \rho U, \rho U \otimes U + P \times \mathcal{I}_3, U(\rho \mathcal{E} + P)).$$

For computing approximated solutions of system (65), a first order approximate Godunov scheme is used. Knowing the approximated solution $\mathcal{W}_k^n$ in all the cells $k$ at time $t^n$, the value of the approximated solution at time $t^{n+1} = t^n + \Delta t^n$ is computed tanks to the (explicit) system of equation:

$$\frac{\mathcal{W}_k^{n+1} - \mathcal{W}_k^n}{\Delta t^n} + \frac{1}{|\Omega_k|} \sum_{l \in \mathcal{V}_k} (\mathcal{F}^{cc}(\mathcal{W}_k^n, \mathcal{W}_l^n).n_{kl} \times S_{kl}) = 0, \tag{66}$$

where $\mathcal{V}_k$ denotes the neighboring cells of cell $\Omega_k$ (for internal cells we have $card(\mathcal{V}_k) = 3$ in 2D and $card(\mathcal{V}_k) = 4$ in 3D). The time-step $\Delta t^n$ is computed to fulfill the CFL constraint based on the maximum of the velocity of the pressure waves $(U \pm C)_{kl}^n$ over all the interface $kl$. The numerical fluxes $(\mathcal{W}_R, \mathcal{W}_L) \mapsto \mathcal{F}^{cc}(\mathcal{W}_R, \mathcal{W}_L)$ used in update (66) are those proposed in [5] on the basis of several previous works [27, 41]. They are based on a relaxation approach which it is not detailed here.

We briefly recall here the main property of this scheme that has been used successfully in [23] for out-of-equilibrium two-phase flow simulations using look-up table EOS (which are complex and highly non-linear). The robustness of the relaxation scheme [5] in case of non-linear EOS is an advantage since the mixture pressure law of the model of section 2 is in general not linear even if each gas is modeled by a linear EOS. One of the conclusion of the work presented in [23] is that the relaxation scheme remains as accurate as any accurate approximate Godunov scheme, while being as robust as the Rusanov scheme. The scheme is conservative which enables to preserve at a numerical level the corresponding property of system (65) and it is entropic. Thanks to these two properties we get that:

- no spurious discontinuity appears in the profile of the approximated rarefaction wave,
- shock waves in the approximated solutions converge towards the exact shock waves, and thus the discrete Rankine-Hugoniot relations converge towards the exact Rankine-Hugoniot relations.

These are important points when the aim is to simulate the propagation of pressure waves. Finally, based on the conservative formulation of the scheme, numerical fluxes allow to obtain a maximum principle for the fractions. It is then ensured that during this convection step, the approximated fractions remain in $[0, 1]$.

It is well-known that explicit Godunov-type schemes suffer from drawbacks for low-Mach flows [9]. Indeed, for such schemes an effective convergence-rate of 1 is obtained for the genuinely non-linear waves (shock and rarefaction wave), while the effective convergence-rate for the linearly degenerate waves (contact waves) is only 1/2, see [11]. Furthermore, the time-step is chosen accordingly to a stability constraint based on the speed of the genuinely non-linear waves. For low-velocity contact-waves (with respect to the speed of the genuinely non-linear waves), this time step is then not well-suited and these schemes are inaccurate for these waves. At last, to avoid spurious modes induced by this lack of accuracy, triangular cells in 2D or tetrahedral cells in 3D are mandatory with approximate Godunov explicit schemes [9, 2].

**Remark** *A second order scheme could be built on the basis of the first order numerical fluxes $\mathcal{F}^{cc}$, for instance using a MUSCL scheme with flux limiters. The order of convergence would be increased from 1/2 to 2/3 for the contact wave, and the accuracy on coarse meshes would be improved [11].*

## 3.2 Numerical fluxes for the thermal diffusion

The system of equations associated with the thermal diffusion effects is:

$$\begin{cases} \partial_t(\rho y_i) = 0, \quad i = 1..3, \\ \partial_t(\rho z_i) = \frac{1}{e}(\nabla \cdot (D_i \nabla(T_i)) - z_i \mathcal{D}), \quad i = 1..3, \\ \partial_t(\rho) = \partial_t(\rho U) = 0, \\ \partial_t(\rho \mathcal{E}) = \mathcal{D}. \end{cases} \tag{67}$$

In that form, accounting for the diffusion operator for the energy fractions $z_i$ is not straightforward, in particular for maintaining the discrete values of $z_i$ in $[0, 1]$. On the basis of section 2.1.6, it is more convenient to rewrite system (67) using equations (36) and the internal energy of each gas:

$$\begin{cases} \partial_t(\rho y_i) = 0, \quad i = 1..3, \\ \partial_t(\rho_i e_i) = \nabla \cdot (D_i \nabla(T_i)), \quad i = 1..4, \\ \partial_t(\rho) = \partial_t(\rho U) = 0. \end{cases} \tag{68}$$

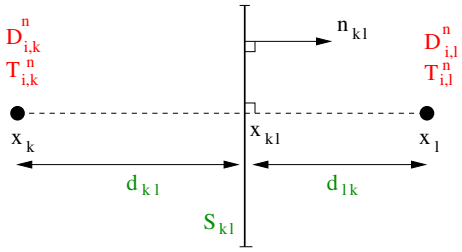


Figure 2: Notation for a given face between to cells $\Omega_k$ and $\Omega_l$. All the notations can be found in figure 1

Indeed, the equation on the mixture energy (i.e. the last equation) of system (67) and the three equations on the energy fractions (i.e. the three equations corresponding to the second line) of system (67), are equivalent to the four equations corresponding to the second line of system (68).

Remembering equation (63), we get in a Finite Volume framework:

$$\frac{(\rho_i e_i)_k^{n+1} - (\rho_i e_i)_k^{n+1}}{\Delta t^n} = \frac{1}{|\Omega_k|} \sum_{l \in \mathcal{V}_k} \left( \mathcal{F}_{i,kl}^{D,n} \times S_{kl} \right), \tag{69}$$

where $\mathcal{F}_{i,kl}^{D,n}$ denotes the numerical thermal flux at the face $kl$, for gas $i$, and computed in an explicit manner. The computation of the numerical thermal fluxes proposed here follows the method described in [35]. The first step consists in computing a numerical thermal flux $\mathcal{F}_{i,kl}^{D,n}$ for each gas $i$ and for each face $kl$ at time-iteration $n$. This computation is performed for each face $kl$ between two cells $\Omega_k$ and $\Omega_l$ and it is an important point to be quoted that:

$$\mathcal{F}_{i,kl}^{D,n} = -\mathcal{F}_{i,lk}^{D,n},$$

so that the conservativity is maintain at a discrete level. Figure 2 recalls some of the notations used here. The thermal flux through face $kl$ is computed thanks to a diffusion coefficient $D_{i,kl}^n$ at the face $kl$ which is a harmonic average of the thermal diffusion coefficients $D_{i,k}^n$ and $D_{i,l}^n$ weighted by the distances $d_{kl}$ and $d_{lk}$:

$$\mathcal{F}_{i,kl}^{D,n} = D_{i,kl}^n \frac{T_{i,k}^n - T_{i,l}^n}{(d_{kl} + d_{lk})/2}, \quad \text{with} \quad \frac{1}{D_{i,kl}^n} = \frac{d_{kl}/D_{i,k}^n + d_{lk}/D_{i,l}^n}{d_{kl} + d_{lk}}, \tag{70}$$

This harmonic averaged introduced for the thermal diffusion coefficient $D_{i,kl}$ allows more stable and accurate approximations when the thermal coefficients strongly fluctuate from one cell to the others. It should be noted that $D_{i,kl}$ can also be written:

$$D_{i,kl}^n = (d_{kl} + d_{lk}) \frac{D_{i,k}^n D_{i,l}^n}{d_{kl} D_{i,l}^n + d_{lk} D_{i,k}^n},$$

so that when only one of the coefficients $D_{i,k}^n$ or $D_{i,l}^n$ is equal to zero, $D_{i,kl}^n$ is also equal to zero. When $D_{i,k}^n = D_{i,l}^n = 0$, the diffusion coefficient $D_{i,kl}^n$ is not correctly defined through the formula above. In these cases, it is then defined equal to zero.

Once the first step is achieved, the internal energies of each gas ($i = 1..4$) are updated by using the numerical thermal fluxes $\mathcal{F}_{i,kl}^{D,n}$ following equation (69). After this update, internal energies of each gas account for the thermal diffusion and it remains to reconstruct the primitive variables of system (67). This is done cell-wise by using their definition:

$$y_{i,k}^{n+1} = y_{i,k}^n, \quad i = 1..3, \tag{71}$$

$$\rho_k^{n+1} = \rho_k^n, \tag{72}$$

$$U_k^{n+1} = U_k^n, \tag{73}$$

$$(\rho e)_k^{n+1} = \sum_{i=1}^{4} (\rho_i e_i)_k^{n+1}, \tag{74}$$

$$(\rho \mathcal{E})_k^{n+1} = (\rho e)_k^{n+1} + \rho_k^{n+1} U^{n+1} \cdot U^{n+1}/2, \tag{75}$$

$$z_{i,k}^{n+1} = \frac{(\rho_i e_i)_k^{n+1}}{(\rho e)_k^{n+1}}, \quad i = 1..3. \tag{76}$$

It should be noted that, if after the update of the internal energies (69) we get $(\rho_i e_i)_k^{n+1} \geq 0$ (see section 2.2.4), then updates (74) and (76) ensure that $(\rho e)_k^{n+1} \geq 0$ and $z_{i,k}^{n+1} \in [0,1]$.

**Remark.** *The density of the mixture, the mass fractions and the velocity field are unchanged, see equations* (71)-(73)*, hence the kinetic energy of each phase and the kinetic energy of the mixture are unchanged by the thermal diffusion during this step of the algorithm.*

**Remark.** *The energy fraction for phase* 4 *is computed from the updated values* $z_{i,k}^{n+1},\ i = 1..3$ *through the energy conservation constraint:*

$$z_{4,k}^{n+1} = 1 - \sum_{i=1}^{3} z_{i,k}^{n+1},$$

*which thanks to equations* (76) *and* (74) *gives:*

$$z_{4,k}^{n+1} = 1 - \frac{\sum_{i=1}^{3} (\rho_i e_i)_k^{n+1}}{(\rho e)_k^{n+1}} = \frac{(\rho_4 e_4)_k^{n+1}}{(\rho e)_k^{n+1}}.$$

*The update* (71)-(76) *is thus consistent with the definition of* $z_4$ *and with energy conservation* $\sum_{i=1}^{4} z_i = 1$.

## 3.3 The source terms and the thermo-chemical equilibrium state

This section is split into two parts. In the first one, a scheme is proposed for solving the ODE associated with the source terms, while in the second part the computation of the equilibrium state that deals with the chemical reaction is explained.

### 3.3.1 Solving the ODE system for the source terms

The ODE system for computing the approximation of the source terms is:

$$\left\{ \begin{array}{l} \partial_t (\rho y_i) = \rho \frac{\overline{y}_i(Y,\tau,e) - y_i}{\lambda}, \quad i = 1..3, \\ \partial_t (\rho z_i) = \rho \frac{\overline{z}_i(Y,\tau,e) - z_i}{\lambda}, \quad i = 1..3, \\ \partial_t (\rho) = \partial_t (\rho U) = \partial_t (\rho \mathcal{E}) = 0. \end{array} \right. \tag{77}$$

System (77) corresponds to a cell-wise time-evolution, cell subscripts are thus omitted here. It can straightforwardly be seen that the velocity, the internal energy and the mass of the mixture are constant: $U(t) = U(t = 0) = U^n$, $e(t) = e(t = 0) = e^n$ and $\rho(t) = \rho(t = 0) = \rho^n$, so that system (77) can be simplified in:

$$\left\{ \begin{array}{l} \partial_t (y_i) = \frac{\overline{y}_i(Y,\tau^n,e^n) - y_i}{\lambda}, \quad i = 1..3, \\ \partial_t (z_i) = \frac{\overline{z}_i(Y,\tau^n,e^n) - z_i}{\lambda}, \quad i = 1..3. \end{array} \right. \tag{78}$$

Since the equilibrium fraction $\overline{Y}$ depends on $Y$, system (78) is a coupled non-linear system of ODE. The function $Y \mapsto \overline{Y}(Y, \tau^n, e^n)$ is non-linear and it is not explicitly known, see 2.1.3. Moreover, the time scale $\lambda$ may depend on $Y$. Solving (78) can thus be a tricky task. Approximated solutions of system (78) are therefore computed by using the approximated system of equations:

$$\left\{ \begin{array}{l} \partial_t (y_i) = \frac{\overline{y}_i(Y^n,\tau^n,e^n) - y_i}{\lambda^n}, \quad i = 1..3, \\ \partial_t (z_i) = \frac{\overline{z}_i(Y^n,\tau^n,e^n) - z_i}{\lambda^n}, \quad i = 1..3, \end{array} \right. \tag{79}$$

which corresponds to system (78) with frozen values for $\overline{Y}$ and $\lambda$. The solutions of system (79) can be explicitly written since the six equations of (79) are linear and independent:

$$Y(t) = Y^n \exp(-t/\lambda^n) + \overline{Y}(Y^n, \tau^n, e^n)\left(1 - \exp(-t/\lambda^n)\right). \tag{80}$$

The time-scale $\lambda^n$ is positive so that in formula (80) the fraction $Y(t)$ is a barycenter of the initial fraction $Y^n$ and of the equilibrium fraction $\overline{Y}(Y^n, \tau^n, e^n)$. As a consequence, if the two latter are in $[0,1]$, $Y(t)$ also belongs to $[0,1]$. Finally, we set: $Y^{n+1} = Y(t = \Delta t^n)$.

The computation of the update of the fractions involves frozen terms, in particular the reaction time-scale $\lambda$. Even if it is stable for any time step, it is mandatory to use time-step $\Delta t^n$ in agreement with $\lambda$ (i.e. $\Delta t^n$ smaller than $\lambda^n$) in order to get an accurate computation of the source terms. In a practical point of view, this is achieved in the overall algorithm because:

- $\Delta t^n$ is related to the speed of propagation of the pressure waves which is large for hydrogen (and even more at high temperatures),
- the method of the *Artificial thickening of the flame* [3] is used, see section 4.2 ; which means that the mesh size, the thermal diffusion coefficients $D_i$ and the reaction time-scale $\lambda$ are controlled.

### 3.3.2 Computing the equilibrium fractions

It remains to describe how the equilibrium fraction $\overline{Y}(Y^n, \tau^n, e^n)$ is computed. We restrict here to the equilibrium case that involves the four gases. It is defined by (21). The other cases can be deduced from this case. First, system (21) is written in intensive form:

$$\left\{\begin{array}{l} T_i(\overline{\tau}_i, \overline{e}_i) = T_4(\overline{\tau}_4, \overline{e}_4),\ \forall i = 1..3, \\ G_1(\overline{\tau}_1, \overline{e}_1) + KG_2(\overline{\tau}_2, \overline{e}_2) - (K+1)G_3(\overline{\tau}_3, \overline{e}_3) = 0, \\ e = \sum_{i=1}^4 \overline{e}_i, \\ \overline{y}_4 = y_4, \\ (\overline{y}_3 - y_3) = -(K+1)\ (\overline{y}_1 - y_1), \\ (\overline{y}_2 - y_2) = K\ (\overline{y}_1 - y_1), \end{array}\right. \tag{81}$$

with $\overline{\tau}_i = \tau/\overline{y}_i$ and $\overline{e}_i = \overline{z}_i e/\overline{y}_i$; and where $e$, $\tau$, $y_i$ and $z_i$, $i = 1..4$, are known. It should be noted that the Gibbs enthalpies are already specific quantities. System (81) then allows to compute $\overline{y}_i$ and $\overline{z}_i$, $i = 1..4$, with respect to $\tau$, $e$ and to the initial mixture fraction $Y$. Thanks to the strict concavity of the mixture entropy, we know from section 2.1.3 that this system possesses at most one solution. If there is no solution for system (81) for a given state $(Y, \tau, e)$, no chemical reaction can occur for this state $(Y, \tau, e)$ and other equilibria should be considered, as described at the end of section 2.1.3.

The temperature equilibrium is a key point for solving system (81). We thus rewrite the latter by switching from the thermodynamical plane $(\tau_i, e_i)$ to the thermodynamical plane $(\tau_i, T_i)$. This yields:

$$\left\{\begin{array}{l} G_1(\overline{\tau}_1, \overline{T}) + KG_2(\overline{\tau}_2, \overline{T}) - (K+1)G_3(\overline{\tau}_3, \overline{T}) = 0, \\ e = \sum_{i=1}^4 \overline{e}_i, \\ \overline{y}_4 = y_4, \\ (\overline{y}_3 - y_3) = -(K+1)\ (\overline{y}_1 - y_1), \\ (\overline{y}_2 - y_2) = K\ (\overline{y}_1 - y_1), \end{array}\right. \tag{82}$$

where $\overline{T}$ is the temperature at equilibrium $\overline{T} = T_i$, $i = 1..4$. Thanks to its definition, $\overline{\tau}_i$ only depends on $\overline{y}_i$. Moreover, the third, forth and fifth equations of (82) explicitly give $\overline{y}_i$, $i = 1..3$, with respect to the sole fraction $\overline{y}_1$. Hence, with a slight abuse of notation, the first equation of (82) can be written as a function of $\overline{T}$ and $\overline{y}_1$:

$$G_1(\overline{y}_1, \overline{T}) + KG_2(\overline{y}_1, \overline{T}) - (K+1)G_3(\overline{y}_1, \overline{T}) = 0. \tag{83}$$

Up to now, no assumption has been made for the EOS except those introduced in section 2.1 dedicated to the building of the model. **Let us now assume that for each gas the internal energy only depends on the temperature and not on the pressure or density:** $T_i \mapsto e_i(T_i)$. This is for instance the case for the most currently used EOS for hydrogen combustion: the Perfect gas EOS and a Chemkin EOS.

The conservation of the energy through the relaxation process (see section 2.1.3, for instance system (21)) gives:

$$\sum_{i=1}^4 y_i e_i(T_i) = e = \overline{e} = \sum_{i=1}^4 \overline{y}_i e_i(\overline{T}).$$

Then, thanks to the last three equations of (82), we can obtain explicitly the equilibrium fraction $\overline{y}_1$ as a function of $\overline{T}$:

$$\overline{y}_1(\overline{T}) = \frac{e - (y_2 - Ky_1)e_2(\overline{T}) - (y_3 + (1+K)y_1)e_3(\overline{T}) - y_4 e_4(\overline{T})}{e_1(\overline{T}) + Ke_2(\overline{T}) - (1+K)e_3(\overline{T})}. \tag{84}$$

Obviously, $\overline{y}_1(\overline{T})$ may not belong to $[0,1]$ depending on the chosen EOS. For Chemkin EOS, $\overline{T} \mapsto \overline{y}_1(\overline{T})$ is an increasing function and $\overline{y}_1(\overline{T}) \in [0,1]$ for a range of temperatures $\overline{T} \in [\overline{T}_m; \overline{T}_M]$ where the temperature $\overline{T}_m$ is such that:

$$\overline{y}_1(\overline{T}_m) = \min(y_1 + y_3/(K+1), 1), \tag{85}$$

and the temperature $\overline{T}_M$ is such that:

$$\overline{y}_1(\overline{T}_M) = \max(y_1 - y_2/K, 0). \tag{86}$$

These boundaries are the intensive counterpart of the bounds of the interval $\mathcal{I}_{\overline{M}_1}$ defined by (20) in section 2.1.3. The temperatures $\overline{T}_m$ and $\overline{T}_M$ have to be computed through equations (85) and (86) which are non

linear. In a practical point of view, this requires the use of a dichotomy algorithm or quasi-Newton methods.

For Perfect Gas EOS, the heat capacity of each gas is a constant and computations of $\overline{T}_m$ and $\overline{T}_M$ are simplified. It can also be convenient to solve the equilibrium by finding $\overline{y}_1$ instead of $\overline{T}$. An algorithm is proposed in appendix 6.2 for the Perfect Gas EOS. For the latter, the computation of the counterpart of the computations of $\overline{T}_m$ and $\overline{T}_M$ can be done explicitly, which save a little of CPU time during the simulations. For the simulations presented in section 4, we have thus retained the Perfect Gas EOS and the algorithm of appendix 6.2.

**Remark.** *For more general EOS, it may be impossible to write explicitly the fraction $\overline{y}_1$ with respect to $\overline{T}$. Finding the equilibrium fraction is thus based on the computation of a non-linear system composed of equation* (83) *and of the equation of energy conservation:*

$$e = \sum_{i=1}^{4} \overline{y}_i e_i \left(\overline{y}_1, \overline{T}\right).$$

*It should be noted that in the equation above, a slight abuse of notation is used and the last three equations of* (82) *have been used for expressing $\overline{y}_i$, $i = 2..4$ with respect to $Y$ and $\overline{y}_1$. Computing approximated solutions of this system of two equations and two unknowns, $\overline{y}_1$ and $\overline{T}$, requires the use of robust quasi-Newton methods.*

# 4 Simulations of laminar deflagration waves

In the present section, some simulations are performed with the model built in section 2 and using the numerical methods described in section 3. The first test case simply corresponds to the validation of the choice of the EOS parameters and of the resulting equilibirum state. In the second set of tests, the classical method of *artificial thickening of the flame* is assessed. It allows to choose the parameters for the third simulation which mimics the experiments DIMITRHY. All these simulations are performed using Perfect Gas EOS and with the same set of parameters which can be found in appendix 6.3. It should be noted that the final aim of the present work is to perform simulations of deflagration waves in air at ambient conditions $T^0 \sim 293\ K$ and $P^0 \sim 10^5\ Pa$. The parameters of the EOS have thus been chosen for that purpose and the preliminary tests of section 4.1 and 4.2 restrict to ambient conditions. The model and the numerical methods obviously extend to other conditions for laminar deflagrations, but several additional tests should be carried out for assessing the thermodynamic choices.

At last, it should be emphasized that transition to detonation is not accounted for in the model. For hydrogen-air mixtures, the transition from deflagration to detonation can occur between $12\% - 18\%$ up to $59\%$ [38, 30]. Thus, some of the initial conditions used below, in particular in section 4.3, could lead to detonation, which is actually clearly not in the scope of the present work.

## 4.1 Adiabatic, isochoric, and complete combustion (AICC) tests

For this test cases, several mixtures of air and hydrogen are chosen for an initial temperature of $T^0 = 293\ K$ and an initial pressure of $P^0 = 10^5\ Pa$. The equilibrium state is computed for each of these initial conditions for Perfect Gas EOS with the parameters of appendix 6.3. For this computation, the initial energy, volume and mass are conserved but, if a reaction occurs, the complete combustion make the pressure and the temperature increase. The simulation results are then compared to the experimental measurements reported in [39]. This comparison can be found in figures 3. In these figures, if reaction does not occur for a given $H_2$ molar-fraction, the AICC pressure and temperature are respectively equal to $P^0$ and $T^0$.

It can be shown in figure 3 that the agreement is satisfactory, even if some differences can be observed. First, the AICC pressure is slightly over-estimated for all the fractions leading to a reaction. The lower flammability limit at 5% of $H_2$ seems well retrieved despite the lack of experimental points around that value, whereas the upper flammability limit differs from 78% of $H_2$ for the experiments to 76% of $H_2$ for the numerical computations. At last, it should be noted that the maximum of the AICC pressure has been measured for a molar fraction of $H_2$ of $\sim 32\%$, whereas for the numerical predictions it arises at $\sim 36\%$. As a conclusion, the results are satisfactory considering the use of Perfect Gas EOS, at least for ambient conditions.

## 4.2 Artificial thickening of the flame front and the burning velocity

Two main ingredients are on the basis of the propagation of the flame front into the fresh gases: the Arrhenius-type law which gives the reaction rate $1/\lambda$ with respect to the temperature of the unburnt gases, and the thermal diffusion that allows to transfer heat from the burnt gases to the unburnt gases. This heat transfer leads to

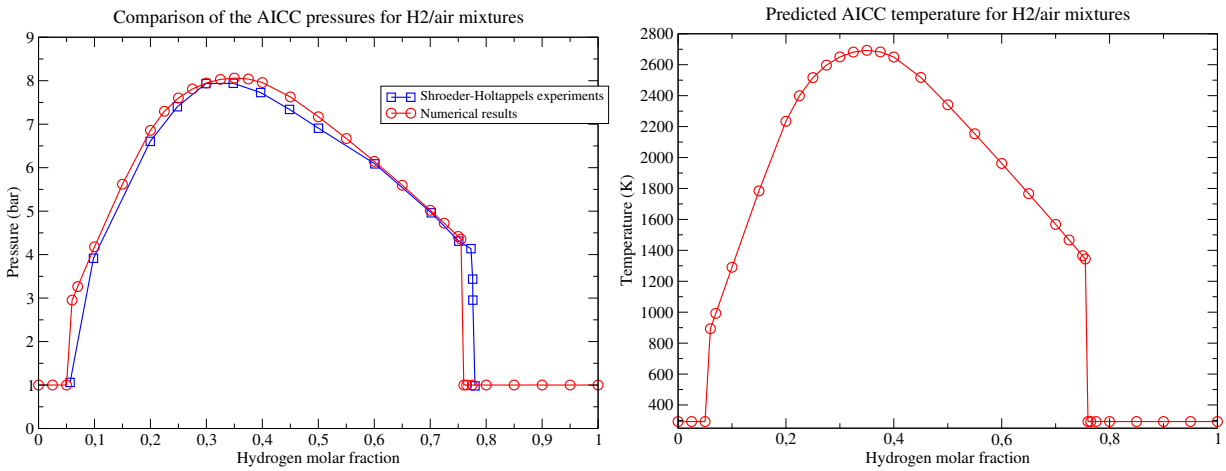


Figure 3: *Left*: Comparison of the AICC pressure predicted by the model and the experimental measurements reported in [39]. *Right*: AICC temperature predicted by the model.

an increase of the temperature in the unburnt gases, which in turns activates the chemical reaction. The front between burnt and unburnt thus propagates from the former to the latter. For deflagration waves, the velocity of the front of the flame is thus given by the balance between the reaction rate law and the thermal diffusion coefficient.

The thermal diffusion coefficient of the gases is small, so that for industrial meshes (as those retained for the test case of section 4.3 for instance) the mesh size remains large with respect to the thermal diffusion scale. In particular, when using first-order scheme for the convection terms, numerical diffusion effects predominate over physical thermal diffusion over a wide range of industrial meshes. When the real physical diffusion coefficients are used in the simulation, the speed of propagation of the flame is then linked to the numerical diffusion, and it is thus not correct.

A technique has early been proposed to bypass this numerical difficulty: the *artificial thickening of the flame front* [3]. This technique is classical and widely used in the combustion community. The key point of this technique is that recovering the correct speed of propagation of the front is the most important feature for the simulations. Hence, when the mesh is too large to account for the physical value of the diffusion coefficient $\mathcal{D}_i$ (i.e. numerical diffusion would prevails), it is replaced by an artificially higher value of the diffusion coefficient $\mathcal{D}_i^{artificial}$ and the reaction time-scale is proportionally increased:

$$\mathcal{D}_i \longrightarrow \mathcal{D}_i^{artificial} \quad \text{and} \quad \lambda \longrightarrow \lambda^{artificial} = \lambda \frac{\mathcal{D}_i}{\mathcal{D}_i^{artificial}}.$$

The reaction time-scale $\lambda$ roughly represents the inverse of the reaction rate. As we focus here on preparing the parameters for the test case of section 4.3, the technique is slightly simplified. The reaction time scale $\lambda$ is fixed and the influence of the value of the diffusion coefficients is studied for mesh sizes that will be used for the test case of section 4.3.

Let us describe the test cases for studying the front propagation. The computational domain is $x \in [0, 1]$ and it is discretized with uniform meshes. The initial pressure and temperature in the domain are respectively $P^0 = 10^5\ Pa$ and $T^0 = 293\ K$; and we only consider here a mixture of air and $H_2$ with 40% $H_2$. These choices have been made in order to choose the parameters for the test case of section 4.3. The ignition of the gases follows the method proposed in [32] for simulating the effect of a spark. Ignition occurs at $x = 0$, the flame front then propagates towards the right part of the domain. Several values for the diffusion coefficients are tested on three different meshes with a mesh size of: 1 $mm$, 2 $mm$ and 4 $mm$.

For each simulation the velocity of the flame front is estimated by the mean of two monitoring points located at $x_a = 0.3\ m$ and $x_b = 0.5\ m$. The approximated velocity of the front is: $(x_b - x_a)/(t_b - t_a)$, where $t_a$ and $t_b$ correspond to the instant at which the front reaches respectively $x_a$ and $x_b$. In order to perform some comparisons with the experimental measurements, the burning velocity $S_l^0$ is used. It corresponds to the velocity of the flame front in the reference frame of the velocity in the unburnt gases $U_f$:

$$S_l^0 = (x_b - x_a)/(t_b - t_a) - U_f. \tag{87}$$

It is worth noting that the approximated value of the speed of propagation of the front in equation (87) (i.e. the first term on the right hand side) can also be estimated thanks to the first equation of (51) by reading in the approximated solution the values on both sides of the front. Nevertheless, there are some oscillations in the approximated solutions of the velocity and it seems more accurate to use equation (87) which restricts the number of values to be read in the approximated solutions.

The test cases are performed with a fixed reaction time-scale $\lambda$ (in $s$) and it is chosen equal to:

$$\lambda(T) = \begin{cases} 10^{-4} \ \exp(1762.0/T), & \text{if} \quad T > 815, \\ 10^{30}, \quad \text{otherwise}, \end{cases} \tag{88}$$

where $T$ is the mixture temperature (in $K$) and the temperature parameter 1762 (in $K$) corresponds to the division $E_a/R$ as proposed in [36]. It should be noted that $\lambda$ is a time scale and it follows the inverse of an Arrhenius law, so that there is no minus sign in the exponential term. Moreover, in order to avoid the slow ignition of the unburnt gases at low temperature (the cold barrier limit), the reaction is turned off for temperatures below 815 $K$ as proposed in [21, 22]. Obviously this cutoff temperature should depend on the mixture and it is fixed here since we only consider one mixture. In our case, with 40% of $H_2$ in air, this source term seems satisfactory. Several parameters have thus been fixed, and these choices strongly reduce the cases for which they are relevant. Dealing with more general configurations would require additional work for choosing more precisely these parameters.

The approximated solutions are plotted in figure 4 at instants $t = 0.0116\ s$ and $t = 0.0183$ for a mesh size of 4 $mm$ and a thermal diffusion coefficient of 32 $W/m/K$. The mixture has been ignited at $x = 0$, so that the flame front travels from the burnt gases zone, on the left of the domain, to the unburnt gases zone, on the right of the domain. The thickening of the flame front can clearly be seen as it measures here approximatively $\sim 0.102\ m$. When computing the speed of propagation of the flame in figure 4, one can found approximatively $\sigma \sim 17.78\ m/s$ and $U_f \sim 14.86\ m/s$, which thanks to formula (87) gives $S_l^0 \sim 2.92\ m/s$. In figure 6 the results for $S_l^0$ have been plotted for diffusion coefficient from 5.0 $10^{-3}$ $W/m/K$ and 512 $W/m/K$. At $T^0 = 293\ K$, the physical values for the thermal diffusion are: $\sim 5.0\ 10^{-2}\ W/m/K$ for $O_2$, $N_2$ and $H_2O$, and $\sim 3.5\ 10^{-1}\ W/m/K$ for $H_2$, so that they all belong to the range given above. Figure 5 shows the approximated solution between time $t = 0.01\ s$ and time $t = 0.025\ s$ at the center of the computational domain $x = 0.5\ m$. Some oscillations can be observed on the velocity profile as mentioned above. They are due to multiple wave reflections that occur after the ignition between the flame front and the left boundary condition (which is a wall condition for ensuring the symmetry of the computational domain). The pressure profile also exhibits such oscillations (with a small amplitude) but it clearly appears from figure 5 that the pressure profile is almost constant across the flame front.

It should be noted that depending on the mesh size, an upper limit exists for the diffusion coefficient. Indeed, the diffusion fluxes are computed using an explicit scheme (see section 3.2) and the classical Fourier constraint thus holds. Let us study a simplified setting: the heat equation for a one-dimensional setting and for constant properties, see appendix 6.4. It yields the constraint:

$$\Delta t < \frac{\rho C_v (\Delta x)^2}{2D}, \tag{89}$$

where $\Delta t$ is the time-step, $\Delta x$ the mesh size and $D$ the thermal diffusion coefficient. In our global scheme, the time-step is computed on the basis of the speed of propagation to the pressure waves according to the classical CFL constraint that can roughly be written:

$$\Delta t \leq \frac{\Delta x}{2(|U| + C)}. \tag{90}$$

It is an important point to be quoted that relation (90) does not involve the thermal diffusion. By introducing the time-step arising in relation (90):

$$\Delta t = \frac{\Delta x}{2(|U| + C)}, \tag{91}$$

into equation (89), the limit for $\Delta x$ with respect to $D$ reads:

$$D < \rho(|U| + C) C_v \Delta x. \tag{92}$$

or using a logarithmic scale:

$$\log_{10}(D) = \log_{10}(\rho(|U| + C) C_v) + \log_{10}(\Delta x). \tag{93}$$

If $\Delta x$ is such that (92) (or equivalently (93)) holds, time-step (91) ensures that (89) is fulfilled; otherwise, explicit diffusion fluxes lead to unstable simulations. The analysis leading to relation (93) holds for a simple setting, in particular the first term on the right-hand side. It should be retained for the general setting that we have the limit line:

$$\log_{10}(D) = A + \log_{10}(\Delta x), \tag{94}$$

where $A$ depends on the schemes and on the test case. Thanks to the results of figure 6, $A$ can be computed with the three last points on the right (one point for each mesh of the three meshes) and it has been found that for the present test case:

$$\log_{10}(D) = 5.301 + \log_{10}(\Delta x). \tag{95}$$

It should be noticed that, when using these three points, the slope 1 of the line (95) is almost exactly recovered. Indeed, for the three meshes the computations have been performed with increasing diffusion coefficient $D$ until the approximations become unstable. according to constraint (89).

In order to prepare the test case of the next section, the following remarks can be done on the basis of figure 6.

1. For the lower diffusion coefficients, the numerical diffusion prevails and the burning velocity is thus independent from the diffusion coefficient. The burning velocity $S^0_{l,min}$associated with the numerical diffusion seems to obey the law (at least for the present test case):

$$\log_{10}(S^0_{l,min}) = 2.29 + 0.91\ \log_{10}(\Delta x). \tag{96}$$

2. For high diffusion coefficients (up to the Fourier limit described above), the thermal diffusion prevails and the logarithm of the burning velocity depends almost linearly from the logarithm of the thermal coefficient. **Moreover, it does not depend on the mesh size**. A regression has shown that for the present test case we have:

$$\log_{10}(S^0_l) = 0.20972 + 0.45205\ \log_{10}(D). \tag{97}$$

It can be observed in figure 6 that for the present test case (which includes the initial conditions, the fixed reaction time-scale (88), and the numerical schemes), a range of thermal coefficient can be found for which the resulting burning-velocity does not depend on the three mesh sizes. This range is here $[10^{1.25}; 10^{2.5}]\ W/m/K \sim [18; 316]\ W/m/K$. For the present initial conditions with 40% $H_2$ in air the measured burning velocity is around $2.9\ m/s \sim 10^{0.463}\ m/s$. In figure 6, this burning velocity is obtained for a thermal diffusion of $10^{1.5}\ W/m/K \sim 32\ W/m/K$. By using relation (96), one can obtain that for $D = 32\ W/m/K$, and thus for $S^0_{l,min} = 2.9\ m/s$, the associated mesh size is equal to $\sim 0.0098\ m$. This corresponds to the upper limit of the mesh size for $D = 32\ W/m/K$, above this limit the burning velocity will be over-estimated. Moreover, following relation (95) with $D = 32\ W/m/K$, the minimal mesh size that fulfills the Fourier constraint is $10^{-3.8}\ mm \sim 1.6\ 10^{-4}\ m$. Respecting this lower limit for the mesh size ensures the stability of the approximated solutions with respect to the Fourier constraint.

The value $D = 32\ W/m/K$ is retained in order to perform the test case of the next section while keeping: the time scale (88) and the initial conditions. The mesh should be such that the mesh size belongs to $[0.16, 9.8]\ mm$.

### 4.3 A two-dimensional DIMITRHY-like test case

We consider here a computational domain that mimics the DIMITRHY test case. It is depicted in figure 7. It consists in a vented tank that initially contains a mixture of $H_2$ and air at ambient temperature and pressure. The main difference with the DIMITRHY experiments is the presence of the upper wall on the top of the domain. It has been added here to obtain a symmetrical domain, and thus to reduce the computational domain to the lower half part. Moreover, the domain is two-dimensional which also enable to reduce the CPU time of the simulation. As mentioned in section 3, the mesh is composed of triangles to avoid spurious modes in the approximated solution due to the use of an explicit convection scheme at low material velocity (with respect to the speed of sound). Indeed, for this simulation, the Mach number is below 0.1 except when the flame passes through the vent, see figure 8 or 12.

The mesh size is set to 4 $mm$ in the tank and in the front of the vent. It is progressively increased near the lower wall to save some computational time. In this area, the mesh size is then larger than the maximal mesh

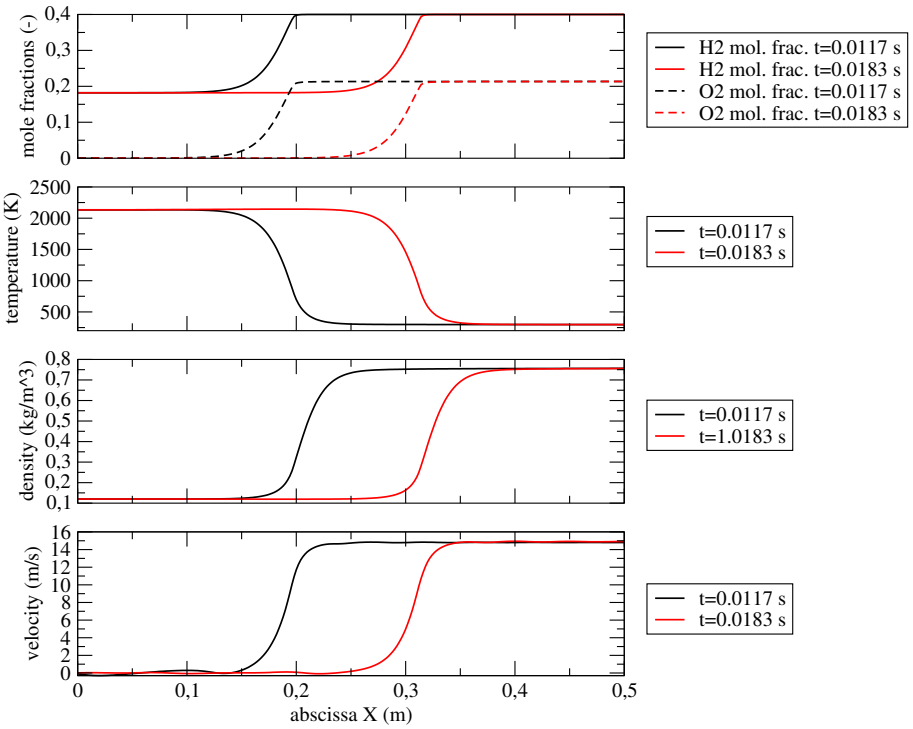


Figure 4: Approximated solution along the first half of the computational domain at time $t = 0.0116\ s$ and time $t = 0.0183\ s$ for a mesh size of 4 $mm$ and a thermal diffusion coefficient of 32 $W/m/K$ (the physical value for $H_2$ should be 5.0 $10^{-2}$ $W/m/K$). Due to the artificial increase of the diffusion coefficient, the flame front is clearly larger than it should be in a physical point of view. The burnt gases are on the left part of the domain, whereas the unburnt gases are on the right part of the domain.

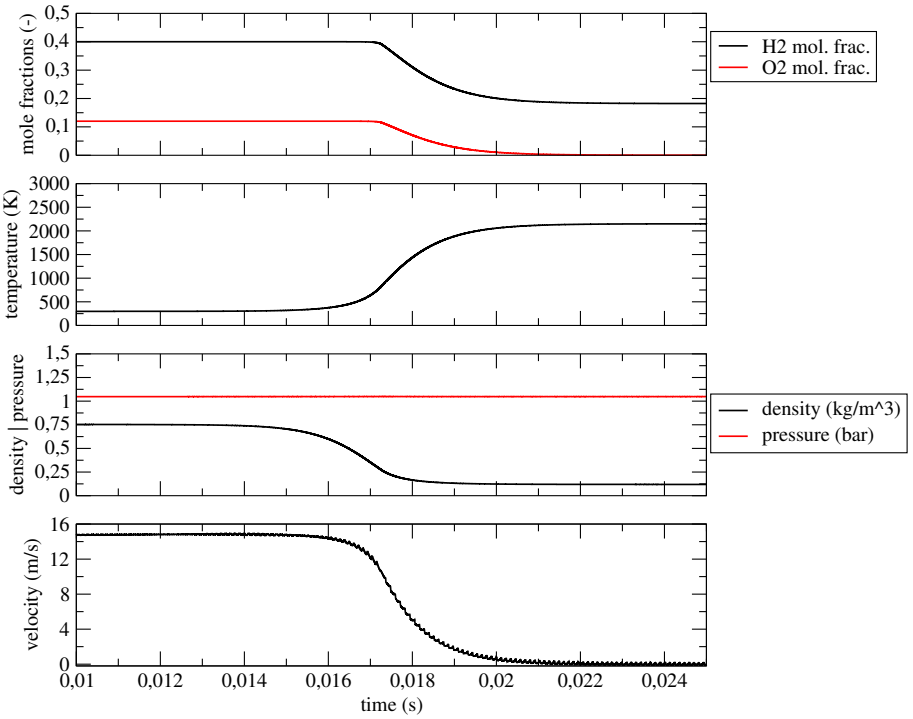


Figure 5: Approximated solution along the time between $t = 0.01\ s$ and $t = 0.025\ s$ at location $x = 0.5\ m$ for a mesh size of 4 $mm$ and a thermal diffusion coefficient of 32 $W/m/K$ (the physical value for $H_2$ should be 5.0 $10^{-2}$ $W/m/K$). It clearly appears that the pressure is almost constant across the flame front, and that oscillations can be observed on the velocity profile.

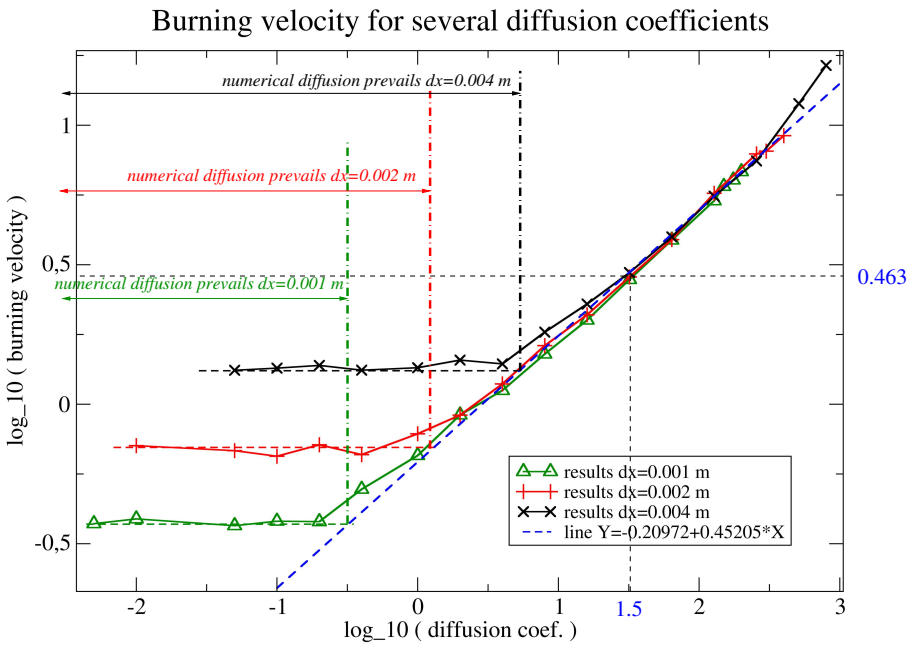


Figure 6: Burning velocities with respect to the thermal diffusion coefficient for three uniform meshes. These results have been obtained with a fixed reaction time scale given by definition (88). The $\log_{10}$-scale is used for the axes. For each meshes, the thermal diffusion coefficients on the left of the vertical dashed-doted line belong to the range for which numerical diffusion prevails. The abscissa for $\log_{10}(32) \sim 1.5$ has been highlighted in blue, together with the associated burning velocity of $\log_{10}(2.9) \sim 0.463$

size of 9.8 $mm$ that has been quoted in the previous section. The burning velocity is thus probably slightly over-estimated near the lower wall. Nevertheless, up to the final time of the simulation, at $T_{fin} = 0.130s$, these parts of the domain are less important.

Figures 9-11 show the approximated solutions for the $H_2$ mole fraction, the $O_2$ mole fraction and the temperature at several instants. Figure 12 presents several quantities at time $t = 0.105621\ s$. On the contrary to the tests of section 4.1, the computational domain is not closed so that energy goes out of the domain by the outlets. The pressure and the temperature can thus not reach their AICC values. On the bulk of the burnt gases, the temperature is around 2100 $K$ even is some hot points clearly appear in the flame. The spatial and time variations of the pressure are less important, and the front flame is almost isobaric. The pressure remains close to the initial pressure and it increases progressively up to $1.5\ 10^5\ Pa$. As expected, the mole fraction of the reactant $H_2$ and $O_2$ are diminished in the burnt gas zone. For mixture with 40% $H_2$ in air, the $O_2$ mole fraction is equal to $60\% \times 1/5 = 12\%$. Hydrogen is thus in excess with respect to $O_2$, and the latter is thus almost entirely consumed in the reaction while only $2 \times 12\%$ of the mole fraction of $H_2$ a required for the reaction. The final mole fractions are then $\sim 0\%$ for $O_2$ (in fact $\sim 7.\ 10^{-6}\%$) and $40\% - 2 \times 12\% = 16\%$ for $H_2$. The simulation results shown in figures 9-11 and 12 are clearly in agreement with these theoretical mole fractions (as in section 4.2).

With the expansion of the flame at the very first stage of the simulation, and the associated pressure increase in the tank, some $H_2$-air mixture is pushed out of the tank through the vent. The propagation of the flame into the fresh gases catches up this expelled unburnt gases which are finally burnt. This pattern is in agreement with the simulation results reported in [42] for a complete DIMITRHY setting. The computation of the burning velocity of the flame on the symmetry line (the upper boundary of the computation domain, see figure 7) according to the technique used in section 4.2 provides a low accuracy because the fluctuations of the velocity fields around the front are important. They are due to the complex reflections and interactions of pressure waves in the tank. Nevertheless, a rough estimate gives a value of $\sim 2.7\ m/s$, which is not too far from the "theoretical" value of 2.9 $m/s$ expected from the previous section.

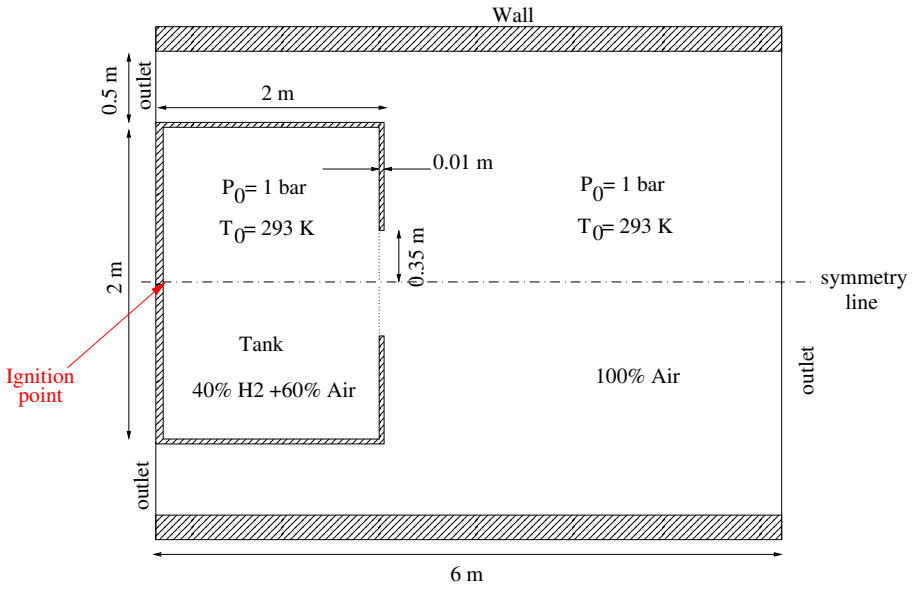


Figure 7: Description of the geometrical domain. Thanks to its symmetry, the computational domain is restricted to the lower half part of this domain.

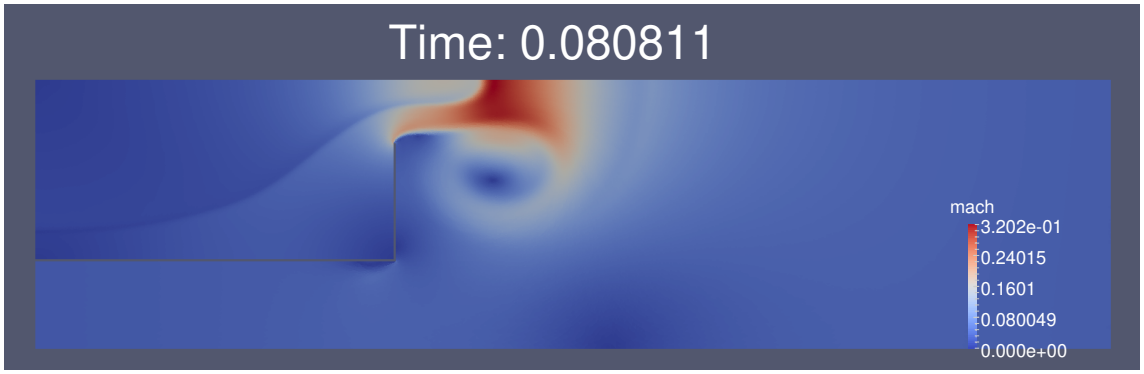


Figure 8: Results for the Mach number when it reaches its maximum over the whole simulation time.

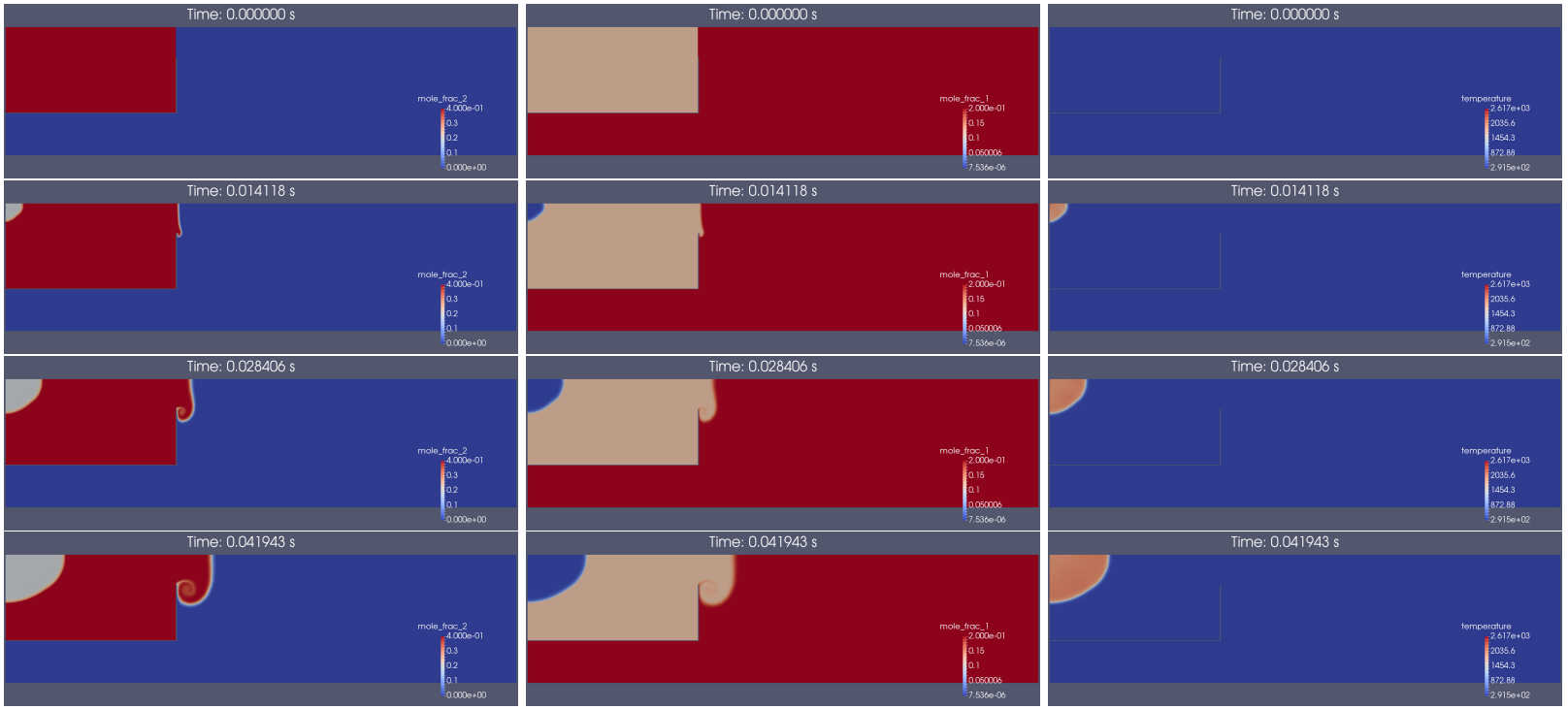


Figure 9: Results for the DIMITRHY-like test case for several instants: the column on the left corresponds to the $H_2$ mole fraction, the column on the center corresponds to the $0_2$ mole fraction, and the column on the right corresponds to the temperature (in $K$).

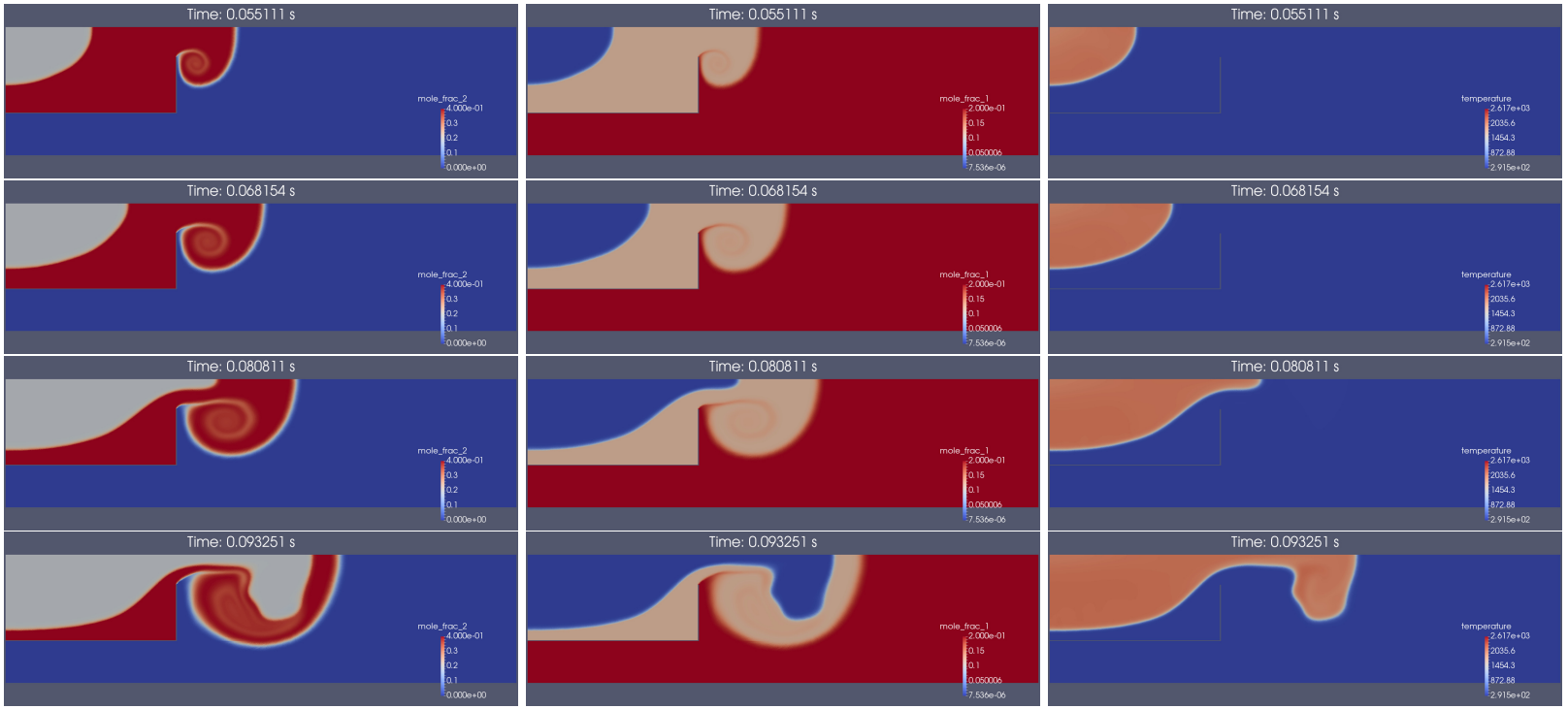


Figure 10: Results for the DIMITRHY-like test case for several instants: the column on the left corresponds to the $H_2$ mole fraction, the column on the center corresponds to the $0_2$ mole fraction, and the column on the right corresponds to the temperature (in $K$).

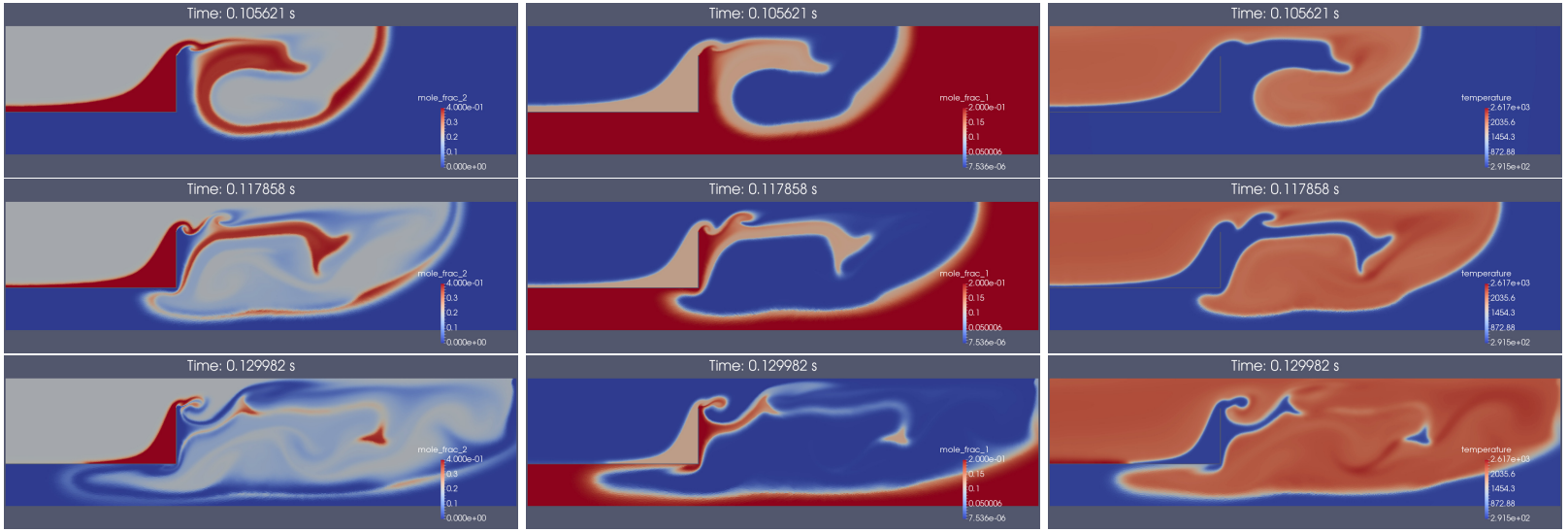


Figure 11: Results for the DIMITRHY-like test case for several instants: the column on the left corresponds to the $H_2$ mole fraction, the column on the center corresponds to the $0_2$ mole fraction, and the column on the right corresponds to the temperature (in $K$).

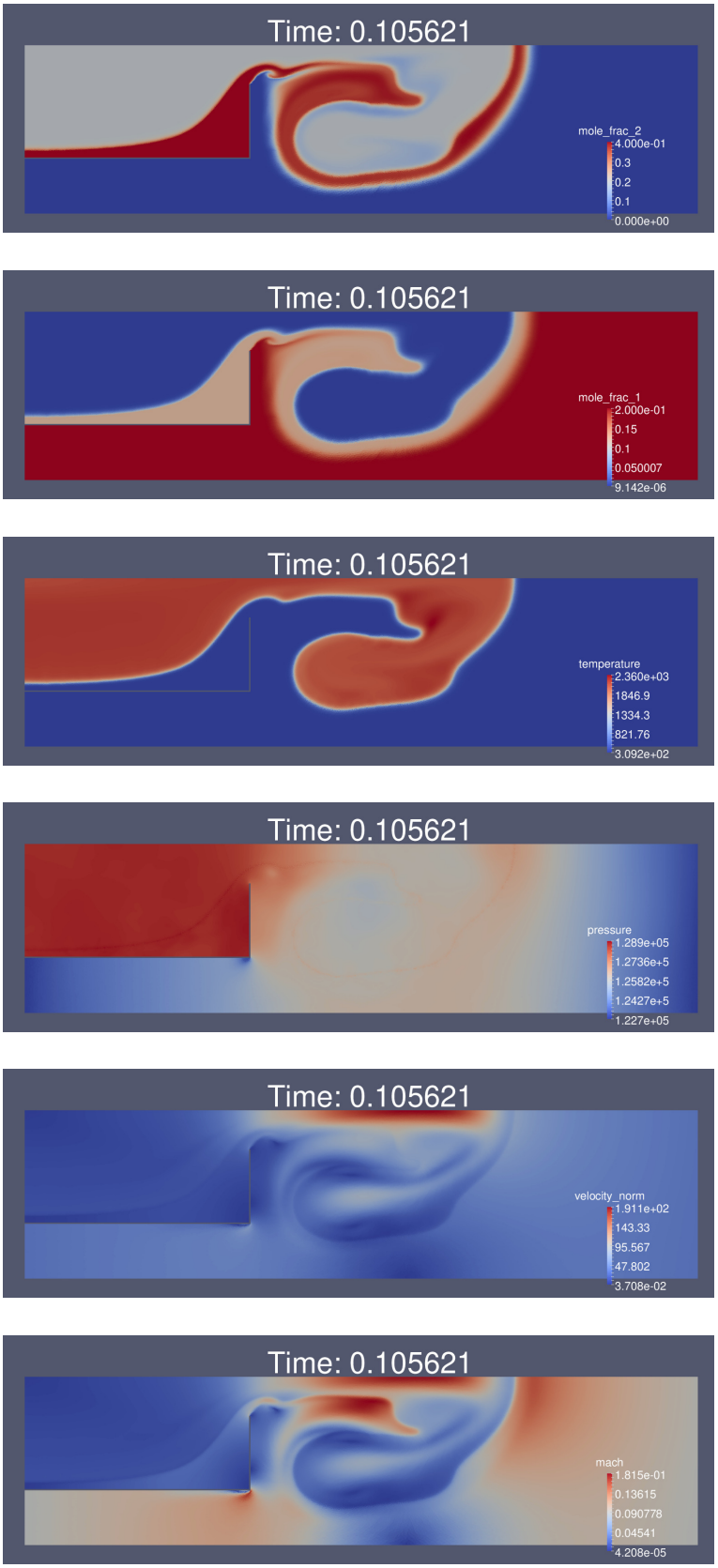


Figure 12: Results for the DIMITRHY-like test at time 0.105621 $s$ and for several variables, from the top to the bottom : $H_2$ mole fraction, $0_2$ mole fraction, temperature (in $K$), pressure (in $Pa$), norm of the velocity field (in $m/s$) and Mach number.

# 5 Conclusion and future directions

In this manuscript, a multi-component multi-temperature model has been presented for simulating laminar deflagration waves in mixtures of four gases: $H_2$, $0_2$, $N_2$ and $H_20$. The model has been built following a thermodynamical approach. Simple numerical schemes and classical methods have been used for assessing the behavior of the model on several basic test cases. The whole is based on classical techniques, in particular the artificial thickening of the flame proposed in [3]. The test case of section 4.3 seems satisfactory and further development are needed in order to perform more realistic simulations of complex industrial studies. Let us enumerate some of these improvements.

- The perfect gas EOS could be sufficient for most of the test cases at ambient pressure and temperature, but the use of the CHEMKIN EOS could improve the numerical results for the AICC conditions and for the flammability limits. In particular, it has been seen in section 4.1 that the upper flammability limit predicted by the model could be improved.

- In section 4.2, the choices of the diffusion coefficient and of the reaction time-scale $\lambda$ have been done in order to get satisfactory results for a $H_2$ mole-fraction of 40% and for a given range of mesh sizes. The study of section 4.2 should be extended in order to propose more general choices for the thermal diffusion coefficient and $\lambda$, by including the dependence to : the initial mixture fractions, the initial pressure and temperature, ... see for instance [7].

- The numerical schemes used in this work are robust but more accurate schemes could be used in order to deal with the low-Mach flows that arise in the deflagration waves. One may for instance quote the pressure-correction schemes (semi-implcit fractional step schemes), see [4, 8, 26, 29, 6] among many others, or the high-order schemes based on high order Taylor expansions.

- At last, turbulence has not been accounted for in the model. Obviously, this aspect should be improved. Turbulence is clearly of key point in the accurate simulation of deflagration waves in industrial settings. The computational domains used for industrial studies are often confined and a lot of different devices may obstruct the propagation of the flame and generate high levels of turbulence. Turbulence modeling through RANS models is known to be a difficult task when considering the classical approaches that have been adapted from those first developed for incompressible flows. In [13], turbulence for compressible flows is considered following thermodynamical point of view and it could be an interesting alternative approach. The increase of the reaction rate due to the turbulence could be accounted for by adding to the thermodynamic temperature a turbulent contribution. Such models remain simple but they possess an interesting mathematical structure that enables to define correctly the shock waves, which is not easy to obtain with the classical RANS approach.

# 6 Appendices

## 6.1 Concavity properties of the entropies

Let us recall some definitions and assumptions of section 2.1.1. We set $\tau_i = V/M_i$, $e_i = E_i/M_i$, $\tau = V/M$ and $e = E/M$. It is assumed that the entropy $s_i$ fulfills the following properties.

- The entropy $s_i$ is strictly concave with respect to $(\tau_i, e_i)$.
- The entropy $s_i$ belongs to $\mathbb{C}^2((\mathbb{R}_*^+)^2)$.
- The partial derivative of $s_i$ with respect to the the specific energy is positive: $\dfrac{\partial s_i}{\partial e_i}_{|\tau_i} > 0$.

On the basis of $s_i$, let us introduce the extensive entropy $\eta_i$:

$$(V_i, M_i, E_i) \mapsto \eta_i(V_i, M_i, E_i) = M_i s_i(V_i/M_i, E_i/M_i). \tag{98}$$

The extensive mixture entropy $\eta$ is then defined as the sum of the extensive entropies $\eta_i$ of each gas: $\eta = \sum_{i=1}^4 \eta_i$. In section 6.1.1 a proof is proposed for the first item $(i)$ of proposition 2.1, while in section 6.1.2 the whole properties of proposition 2.3 are proved.

### 6.1.1 Concavity of the extensive entropy $\eta_i$

Thanks to definition (98) of $\eta_i$, one can easily write the Hessian matrix of $W_i = (V_i, M_i, E_i) \mapsto \eta_i(W_i)$. By keeping the upper triangular part of the matrix (which is symmetric), it reads:

$$M_i\ \eta_i''(V_i, M_i, E_i) = \begin{pmatrix} \dfrac{\partial^2 s_i}{\partial\tau_i\partial\tau_i} & \left(-\tau_i\dfrac{\partial^2 s_i}{\partial\tau_i\partial\tau_i} - e_i\dfrac{\partial^2 s_i}{\partial\tau_i\partial e_i}\right) & \dfrac{\partial^2 s_i}{\partial\tau_i\partial e_i} \\ \cdot & A_{\tau_i,e_i} & \left(-\tau_i\dfrac{\partial^2 s_i}{\partial\tau_i\partial e_i} - e_i\dfrac{\partial^2 s_i}{\partial\tau_i\partial\tau_i}\right) \\ \cdot & \cdot & \dfrac{\partial^2 s_i}{\partial e_i\partial e_i} \end{pmatrix}, \tag{99}$$

where the term on the second line and second column is:

$$A_{\tau_i,e_i} = (\tau_i, e_i)\cdot s_i''\cdot(\tau_i, e_i)^\top,$$

and where $s_i''$ denotes the Hessian matrix of $s_i$ with respect to $(\tau_i, e_i)$, see (43). Then for any vector $(x, y, z)$ we get:

$$M_i\ (x, y, z)\cdot\eta_i''(V_i, M_i, E_i)\cdot(x, y, z)^\top = (x - y\tau_i, z - ye_i)\cdot s_i''(\tau_i, e_i)\cdot(x - y\tau_i, z - ye_i)^\top.$$

Since $s_i$ is (strictly) concave, the equality above implies that for all $(x, y, z) \neq (0, 0, 0)$:

$$(x, y, z)\cdot\eta_i''(V_i, M_i, E_i)\cdot(x, y, z)^\top \leq 0.$$

Nonetheless, despite the strict concavity of $s_i$, the entropy $\eta_i$ can not be strictly concave because its degeneracy manifold, $\{(x, y, z)\ /\ x - y\tau_i = 0,\ z - ye_i = 0\}$, do not reduce to a single point. This complete the proof of the first item of proposition 2.1.

### 6.1.2 Concavity properties of the extensive mixture entropy $\eta$

In this section, we propose to prove the proposition 2.3. For the sake of readability we set $W_i = (V_i, M_i, E_i)$ and $W = (W_1, W_2, W_3, W_4)$.

**Proof for item $(i)$.**
From proposition 2.1, we know that $W_i \mapsto \eta_i(W_i)$ is concave. Since $\eta$ is the sum of the entropies $\eta_i$ and since the variables $(V_i, M_i, E_i)$ are separated for the different $i$, proving the concavity of $\eta$ is straightforward. Let us choose $W$, $W'$, $\lambda \in [0, 1]$ and $\lambda' = 1 - \lambda$. We then have:

$$\eta(\lambda W + \lambda' W') = \sum_{i=1}^4 \eta_i(\lambda V_i + \lambda' V_i', \lambda M_i + \lambda' M_i', \lambda E_i + \lambda' E_i')$$

$$\geq \lambda\sum_{i=1}^4 \eta(V_i, M_i, E_i) + \lambda'\sum_{i=1}^4 \eta(V_i', M_i', E_i') = \lambda\eta(W) + \lambda'\eta(W')$$

The entropy $\eta$ is thus concave with respect to $W$, but it is not strictly concave because of the non-strict concavity of $\eta_i$. This complete the proof of item $(i)$.

**Proof for item** $(ii)$**.**
Let us assume now that the mass fractions $M_i/M = a_i^0$ and energy fractions $E_i/E = b_i^0$ are fixed for all the gases. The entropy can then be written:

$$\frac{\eta}{M}\left((a_i^0, b_i^0)_{i=1..4}, \tau, e\right) = \sum_{i=1}^{4} a_i^0 s_i \left(\frac{\tau}{a_i^0}, \frac{e b_i^0}{a_i^0}\right). \tag{100}$$

Let us choose $(\tau, e)$, $(\tau', e')$, $\lambda \in [0,1]$ and $\lambda' = 1-\lambda$. The definition of the entropy (100) leads to:

$$\frac{\eta}{M}\left((a_i^0, b_i^0)_{i=1..4}, \lambda\tau + \lambda'\tau', \lambda e + \lambda' e'\right) = \sum_{i=1}^{4} a_i^0 s_i \left(\frac{\lambda\tau + \lambda'\tau'}{a_i^0}, \frac{(\lambda e + \lambda' e') b_i^0}{a_i^0}\right),$$

$$\frac{\eta}{M}\left((a_i^0, b_i^0)_{i=1..4}, \lambda\tau + \lambda'\tau', \lambda e + \lambda' e'\right) = \sum_{i=1}^{4} a_i^0 s_i \left(\lambda\left(\frac{\tau}{a_i^0}\right) + \lambda'\left(\frac{\tau}{a_i^0}\right)', \lambda\left(\frac{e b_i^0}{a_i^0}\right) + \lambda'\left(\frac{e b_i^0}{a_i^0}\right)'\right),$$

which, thanks to the strict concavity of the entropies $(\tau_i, e_i) \mapsto s_i$, gives the inequalities:

$$\frac{\eta}{M}\left((a_i^0, b_i^0)_{i=1..4}, \lambda\tau + \lambda'\tau', \lambda e + \lambda' e'\right) > \lambda \sum_{i=1}^{4} a_i^0 s_i \left(\left(\frac{\tau}{a_i^0}\right), \left(\frac{e b_i^0}{a_i^0}\right)\right) + \lambda' \sum_{i=1}^{4} a_i^0 s_i \left(\left(\frac{\tau}{a_i^0}\right)', \left(\frac{e b_i^0}{a_i^0}\right)'\right),$$

and:

$$\frac{\eta}{M}\left((a_i^0, b_i^0)_{i=1..4}, \lambda\tau + \lambda'\tau', \lambda e + \lambda' e'\right) > \lambda \frac{\eta}{M}\left((a_i^0, b_i^0)_{i=1..4}, \tau, e\right) + \lambda' \frac{\eta}{M}\left((a_i^0, b_i^0)_{i=1..4}, \tau', e'\right). \tag{101}$$

Hence, relation (101) proves that the entropy $(\tau, e) \mapsto \frac{\eta}{M}\left((a_i^0, b_i^0)_{i=1..4}, \tau, e\right)$ is strictly concave. This complete the proof of item $(ii)$.

**Proof for item** $(iii)$**.**
We use here the equality $V_i = V$ and the fact that $V$ is supposed constant. Indeed, the entropy per unit of volume $\sigma_i$ (in $J/K/m^3$) is introduced: $(\rho_i, \epsilon_i) \mapsto \sigma_i(\rho_i, \epsilon_i) = \rho_i s_i(1/\rho_i, \epsilon_i/\rho_i)$, where $\epsilon_i = \rho_i e_i$ is the internal energy per unit of volume (in $J/m^3$). It can be proved that:

$$(\rho_i, \epsilon_i) \mapsto \sigma_i \quad \text{strictly concave} \quad \Longleftrightarrow \quad (\tau_i, e_i) \mapsto s_i \quad \text{strictly concave} \quad ,$$

see for instance [17, 28, 34]. It should be noted that from the definition of $\sigma_i$ we get $M_i s_i = V\sigma_i$. So that, by introducing the mass and energy conservation: $M_4 = M - \sum_{i=1}^{3} M_i$ and $E_4 = E - \sum_{i=1}^{3} E_i$, the mixture entropy then reads:

$$\eta\left((M_i, E_i)_{i=1..3}, V, M, E\right) = V \sum_{i=1..3} \sigma_i \left(\frac{M_i}{V}, \frac{E_i}{V}\right) + V\sigma_4 \left(\frac{M - \sum_{i=1}^{3} M_i}{V}, \frac{E - \sum_{i=1}^{3} E_i}{V}\right).$$

The computation of the Hessian matrix of $\eta$ with respect to $(M_i, E_i)_{i=1..3}$ for fixed $(V, M, E)$ is then straightforward and we finally obtain the relation:

$$V\ \eta''\left((M_i, E_i)_{i=1..3}\right) = \sum_{i=1}^{4} \sigma_i''(\rho_i, \epsilon_i).$$

Hence, the strict concavity of $(\rho_i, \epsilon_i) \mapsto \sigma_i$ implies the strict concavity of $((M_i, E_i)_{i=1..3}) \mapsto \eta$. Since $(V, M, E)$ are fixed, we finally get the strict concavity of $((M_i/M, E_i/E)_{i=1..3}) \mapsto (\eta/M)$. This complete the proof of item $(iii)$.

## 6.2 Algorithm for computing the equilibrium fractions in the case of Perfect Gas EOS

In this section we describe a simple algorithm for computing the equilibrium fractions when all the gases obey a Perfect Gas law. For such EOS we have $C_{v,i} T_i = e_i - Q_i$, where $Q_i$ is an activation energy (constant) and where the heat capacity $C_{v,i}$ is a constant. The temperature equilibrium, $\overline{T} = T_i =$, $i = 1..4$, leads to:

$$\overline{z}_i e = \overline{y}_i (C_{v,i} T_i + Q_i) = \overline{y}_i (C_{v,i} \overline{T} + Q_i).$$

By summing the relations above over the gases $i$, and using the second relation of (82) we obtain:

$$e = \overline{T} \sum_{i=1}^{4} (\overline{y}_i C_{v,i}) + \sum_{i=1}^{4} (\overline{y}_i Q_i),$$

or equivalently:

$$\overline{T} = \frac{e - \sum_{i=1}^{4} (\overline{y}_i Q_i)}{\sum_{i=1}^{4} (\overline{y}_i C_{v,i})}. \tag{102}$$

The equilibrium temperature $\overline{T}$ is therefore a function of the equilibrium mass fractions, and thus thanks to the third, forth and fifth equations of (82), we finally get $\overline{T}$ as a function of the sole fraction $\overline{y}_1$: $\overline{y}_1 \mapsto \overline{T}(\overline{y}_1)$. If we introduce this relation into relation (83), we obtain a non-linear equation on $\overline{y}_1$:

$$G_1(\overline{y}_1, \overline{T}(\overline{y}_1)) + KG_2(\overline{y}_1, \overline{T}(\overline{y}_1)) - (K+1)G_3(\overline{y}_1, \overline{T}(\overline{y}_1)) = 0. \tag{103}$$

The solution $\overline{y}_1$ of equation (103) should be such that $\overline{y}_i \in [0,1]$. By using the last three relations of system (82) then implies that $\overline{y}_1 \in [\max(0, y_1 - y_2/K), \min(1, y_1 + y_3/(K+1))]$, see the definition of the interval (20). In a practical point of view, if it exists, the solution of problem (103) is unique and computed by the mean of a dichotomy algorithm or quasi-Newton method on $[\max(0, y_1 - y_2/K), \min(1, y_1 + y_3/(K+1))]$. When a solution of equation (103) exists, all the other quantities can be computed from $\overline{y}_1$.

## 6.3 Parameters for the Perfect Gas EOS

The specific entropy (in $J/K/kg$) of the Perfect Gas reads:

$$s_i(\tau_i, e_i) = C_{v,i} \ln \left( (e_i - Q_i) \tau_i^{(\gamma_i - 1)} \right) + s_i^0,$$

where $C_{v,i}$ is the specific heat capacity (in $J/K/kg$), $Q_i$ is an activation energy (in $J/kg$), $\gamma_i$ is the polytropic coefficient and $s_i^0$ is a reference entropy (in $J/K/kg$). The parameters of the Perfect Gas EOS used for the simulations of section 4 are gathered in the following table:

| | $O_2$ $(i=1)$ | $H_2$ $(i=2)$ | $H_2O$ $(i=3)$ | $N_2$ $(i=4)$ |
|---|---|---|---|---|
| $C_v$ | $7.99782\ 10^2$ | $1.06338\ 10^4$ | $2.11931\ 10^3$ | $8.42721\ 10^2$ |
| $\gamma$ | 1.32895 | 1.39323 | 1.21827 | 1.35678 |
| $Q$ | $1.39353\ 10^7$ | $9.44682\ 10^6$ | 0 | $2.80134\ 10^{-2}$ |
| $s^0$ | $1.53234\ 10^3$ | $-1.06945\ 10^5$ | $-1.53883\ 10^4$ | $1.33096\ 10^3$ |
| $\mathcal{M}$ | $31.9988\ 10^{-3}$ | $2.01588\ 10^{-3}$ | $1.801528\ 10^{-2}$ | $28.0134\ 10^{-3}$ |

The last line of the previous table gives the molar masses (in $kg/mole$) of each gas. The latter are used for computing the parameter $K$ and for translating mass fractions into molar fractions (and conversely). We obviously have $\mathcal{M}_1/2 + \mathcal{M}_2 = \mathcal{M}_3$.

## 6.4 The heat equation and the Fourier constraint

Let us consider the heat equation with a constant density $\rho$, a constant heat capacity $C_v$ and a constant thermal diffusion coefficient $D$:

$$\rho C_v \partial_t (T) = D \partial_x^2 (T).$$

By applying a first-order finite-difference scheme to the equation above with constant and uniform mesh size $\Delta x$ and time step $\Delta t$, the approximated temperatures $T_i^n$ in the cells $i$ at iteration $t^n$ allow to compute the approximated temperatures at iteration $t^{n+1} = t^n + \Delta t$ through the update:

$$T_i^{n+1} - T_i^n = a(T_{i+1}^n - 2T_i^n + T_{i-1}^n), \quad \text{with} \quad a = \frac{D\Delta t}{\rho C_v (\Delta x)^2}.$$

or by re-arranging the terms:

$$T_i^{n+1} = aT_{i+1}^n + (1-2a)T_i^n + aT_{i-1}^n. \tag{104}$$

In this relation, $a > 0$ and the sum of the coefficients on the right hand side are equal to 1. Thus, if $1 - 2a > 0$ the temperature $T_i^{n+1}$ is a barycenter of the temperature in the neighboring cells at iteration $n$. As a consequence,

if for all $i$ we have $T_i^n \in [T_{min}^n, T_{max}^n]$, then $T_i^{n+1}$ also belong to $[T_{min}^n, T_{max}^n]$. Moreover, relation (102) gives for the increment between to cells $i$ and $i-1$:

$$(T_i^{n+1} - T_{i-1}^{n+1}) = a(T_{i+1}^n - T_i^n) + (1-2a)(T_i^n - T_{i-1}^n) + a(T_{i-1}^n - T_{i-2}^n).$$

If one assumes that the approximated solution at iteration $n$ is monotonically increasing (resp. decreasing), the condition $1-2a > 0$ ensures that the approximated solution at iteration $n+1$ is also monotonically increasing (resp. decreasing). Therefore, we deduce from the classical results given in [20] that the scheme is TVD under the constraint $1-2a > 0$. This constraint can also be written:

$$\Delta t < \frac{\rho C_v (\Delta x)^2}{2D}.$$

# References


[1] Thomas Barberon and Philippe Helluy. Finite volume simulation of cavitating flows. *Computers & fluids*, 34(7):832–858, 2005.

[2] Pascal Bruel, Simon Delmas, Jonathan Jung, and Vincent Perrier. A low mach correction able to deal with low mach acoustics. *Journal of Computational Physics*, 378:723–759, 2019.

[3] Daniel T. Butler and Peter J. O'rourke. A numerical method for two dimensional unsteady reacting flows. In *Symposium (international) on combustion*, volume 16, pages 1503–1515. Elsevier, 1977.

[4] V Casulli and D Greenspan. Pressure method for the numerical solution of transient, compressible fluid flows. *International Journal for Numerical Methods in Fluids*, 4(11):1001–1012, 1984.

[5] Christophe Chalons and Jean-François Coulombel. Relaxation approximation of the euler equations. *Journal of Mathematical Analysis and Applications*, 348(2):872–893, 2008.

[6] Alexandre Joel Chorin. Numerical solution of the navier-stokes equations. *Mathematics of computation*, 22(104):745–762, 1968.

[7] Paul Clavin. Dynamic behavior of premixed flame fronts in laminar and turbulent flows. *Progress in energy and combustion science*, 11(1):1–59, 1985.

[8] Phillip Colella and Karen Pao. A projection method for low speed flows. *Journal of Computational Physics*, 149(2):245–269, 1999.

[9] Stéphane Dellacherie. Analysis of godunov type schemes applied to the compressible euler system at low mach number. *Journal of Computational Physics*, 229(4):978–1016, 2010.

[10] Alexandre Ern and Vincent Giovangigli. Impact of detailed multicomponent transport on planar and counterflow hydrogen/air and methane/air flames. *Combustion science and technology*, 149(1-6):157–181, 1999.

[11] Thierry Gallouët, J-M Hérard, and Nicolas Seguin. Some recent finite volume schemes to compute euler equations using real gas EOS. *International journal for numerical methods in fluids*, 39(12):1073–1138, 2002.

[12] Bassam Gamal, Laura Gastaldo, and Denis Veynante. The CALIF 3 S-P 2 REMICS software: simulation of accelerated deflagrations using RANS and LES approaches. In *10th European Combustion Meeting*, pages 1201–1206, Napoli (virtual conference), Italy, April 2021.

[13] Sergey Gavrilyuk, Jean-Marc Hérard, Olivier Hurisse, and Ali Toufaili. Theoretical and numerical analysis of a simple model derived from compressible turbulence. *Journal of Mathematical Fluid Mechanics*, 24(2):1–34, 2022.

[14] AS GexCon. FLACS v10 .4 user's manual. *GexCon AS: Bergen, Norway*, 2009.

[15] Vincent Giovangigli. Mathematics of thermochemistry. In *Multicomponent Flow Modeling*, pages 119–156. Springer, 1999.

[16] Vincent Giovangigli. Multicomponent flow modeling. *Science China Mathematics*, 55(2):285–308, 2012.

[17] Edwige Godlewski and Pierre-Arnaud Raviart. *Hyperbolic systems of conservation laws*. Number 3-4. Ellipses, 1991.

[18] David G Goodwin, Harry K Moffat, and Raymond L Speth. Cantera: An object-oriented software toolkit for chemical kinetics, thermodynamics, and transport processes. *Caltech, Pasadena, CA*, 124, 2009.

[19] Olav Roald Hansen, J Renoult, MP Sherman, and SR Tieszen. Validation of FLACS-hydrogen CFD consequence prediction model against large scale H2 explosion experiments in the FLAME facility. 2005.

[20] Amiram Harten, Peter D Lax, and Bram van Leer. On upstream differencing and godunov-type schemes for hyperbolic conservation laws. *SIAM review*, 25(1):35–61, 1983.

[21] Longting He and Paul Clavin. Premixed hydrogen-oxygen flames. Part I: Flame structure near the flammability limits. *Combustion and flame*, 93(4):391–407, 1993.

[22] Longting He and Paul Clavin. Premixed hydrogen-oxygen flames. Part II: Quasi-isobaric ignition near the flammability limits. *Combustion and Flame*, 93(4):408–420, 1993.

[23] Philippe Helluy, Olivier Hurisse, and Lucie Quibel. Assessment of numerical schemes for complex two-phase flows with real equations of state. *Computers & Fluids*, 196:104347, 2020.

[24] Olivier Hurisse. BGK source terms for out-of-equilibrium two-phase flow models. *Continuum Mechanics and Thermodynamics*, pages 1–17, 2022.

[25] Olivier Hurisse and Lucie Quibel. Simulations of water-vapor two-phase flows with non-condensable gas using a noble-able-chemkin stiffened gas equation of state. *Computers & Fluids*, page 105399, 2022.

[26] Raad I Issa. Solution of the implicitly discretised fluid flow equations by operator-splitting. *Journal of computational physics*, 62(1):40–65, 1986.

[27] Shi Jin and Zhouping Xin. The relaxation schemes for systems of conservation laws in arbitrary space dimensions. *Communications on pure and applied mathematics*, 48(3):235–276, 1995.

[28] Jonathan Jung. *Schémas numériques adaptés aux accélérateurs multicoeurs pour les écoulements bifluides.* Theses, Université de Strasbourg, October 2013.

[29] KC Karki and SV Patankar. Pressure based calculation procedure for viscous flows at all speeds in arbitrary configurations. *AIAA journal*, 27(9):1167–1174, 1989.

[30] Kuo K.K. *Principles of Combustion.* John Wiley & Sons, New York, second edition, 2005.

[31] Alexander A Konnov. Remaining uncertainties in the kinetic mechanism of hydrogen combustion. *Combustion and flame*, 152(4):507–528, 2008.

[32] Guilhem Lacaze. *Simulation aux Grandes Echelles de l'allumage de moteurs fusées cryotechniques.* PhD thesis, Toulouse, INPT, 2009.

[33] NM Marinov, CK Westbrook, and WJ Pitz. Detailed and global chemical kinetics model for hydrogen. *Transport phenomena in combustion*, 1:118, 1996.

[34] Hélène Mathis. A thermodynamically consistent model of a liquid-vapor fluid with a gas. *ESAIM: Mathematical Modelling and Numerical Analysis*, 53(1):63–84, 2019.

[35] Sébastien Perron, Sylvain Boivin, and Jean-Marc Hérard. A finite volume method to solve the 3D navier–stokes equations on unstructured collocated meshes. *Computers & fluids*, 33(10):1305–1333, 2004.

[36] Pierre Quillatre. *Simulation aux grandes échelles d'explosions en domaine semi-confiné.* PhD thesis, 2014.

[37] Antonio L Sánchez and Forman A Williams. Recent advances in understanding of flammability characteristics of hydrogen. *Progress in Energy and Combustion Science*, 41:1–55, 2014.

[38] Dorofeev S.B., Sidorov V.P., Kuznetsov M.S., Matsukov I.D., and Alekseev V.I. Effect of scale on the onset of detonations. *Shock Waves*, 10:137–149, 2000.

[39] Volkmar Schröder and Kai Holtappels. Explosion characteristics of hydrogen-air and hydrogen-oxygen mixtures at elevated pressures. 2005.

[40] Joel Smoller. *Shock waves and reaction—diffusion equations*, volume 258. Springer Science & Business Media, 2012.

[41] I Suliciu. On the thermodynamics of fluids with relaxation and phase transitions. fluids with relaxation. *Internat. J. Engrg. Sci*, 36:921–947, 1998.

[42] Elena Vyazmina, Simon Jallais, Laurent Krumenacker, Amita Tripathi, Alban Mahon, Julien Commanay, Sergey Kudriakov, Etienne Studer, Thomas Vuillez, and F Rosset. Vented explosion of hydrogen/air mixture: An intercomparison benchmark exercise. *international journal of hydrogen energy*, 44(17):8914–8926, 2019.

[43] Forman A. Williams. Combustion theory: the fundamental theory of chemically reacting flow systems. Technical report, 1985.